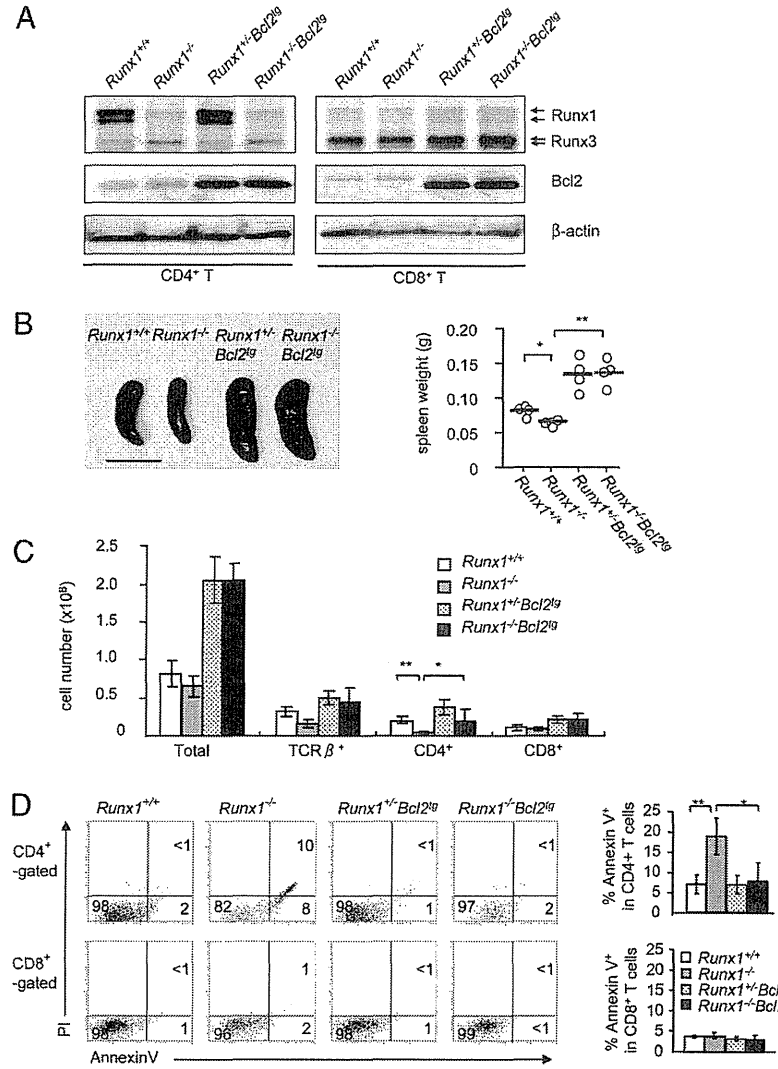

FIGURE 1. Overexpression of *Bcl2* rescues apoptotic *Runx1*-deleted CD4$^+$ T cells. (**A**) Confirmation of *Runx1* deletion and *Bcl2* transgene expression by immunoblot analyses. CD4$^+$ and CD8$^+$ T cells were purified from spleens of 8–12-wk-old *Runx1*$^{+/+}$, *Runx1*$^{-/-}$, *Runx1*$^{+/-}$*Bcl2*^{tg}, or *Runx1*$^{-/-}$*Bcl2*^{tg} mice. Lysates were prepared and processed. β-actin served as a loading control. (**B**) A representative photograph of spleens from 8–12-wk-old mice (*left panel*). Scale bar, 1 cm. Spleen weights of 8–12-wk-old mice (*right panel*; n = 4). *p = 0.01, **p = 0.0003. (**C**) The number of CD4$^+$ T cells increased after *Bcl2* transgene expression. Cell numbers of total, TCRβ$^+$, CD4$^+$, or CD8$^+$ splenocytes from 8–12-wk-old mice (n = 4). *p = 0.046, **p = 0.0004. (**D**) The percentages of apoptotic cells were reduced in the presence of *Bcl2* transgene expression. Flow cytometry analyses of splenocytes derived from 8–12-wk-old mice. Bar graphs show mean (± SD) percentages of annexin V$^+$ cells in the CD4$^+$- or CD8$^+$-gated populations derived from each mouse (n = 4). *p = 0.013, **p = 0.0012.

Lungs from young *Runx1*$^{-/-}$*Bcl2*^{tg} mice scored between 1 and 2, whereas those from aged mice scored up to 3, reflecting the more severe pathology in aged mice. In contrast, lungs from age-matched control mice showed no pathological phenotype and scored 0.

To monitor airway-residing immune cells, BALF was recovered, and the cells in it were analyzed (Fig. 3A, 3B). Strikingly, in aged (but not young) *Runx1*$^{-/-}$*Bcl2*^{tg} mice, ~5-fold greater numbers of BALF cells were detected compared with control littermates. BALF cells from *Runx1*$^{-/-}$*Bcl2*^{tg} mice were composed predominantly of Gr-1$^+$Mac-1$^+$ granulocytes and, to lesser degrees, TCR-β$^+$ T cells, B220$^+$ B cells, and Gr-1$^-$Mac-1$^+$ macrophages. Also, the levels of proinflammatory cytokines, such as IFN-γ and TNF, were ~3-fold higher in BALF from aged *Runx1*$^{-/-}$*Bcl2*^{tg} mice compared with control mice (Fig. 3C). This suggests the occurrence of a cytokine storm in the lungs of aged *Runx1*$^{-/-}$*Bcl2*^{tg} mice.

Systemic inflammation in aged Runx1$^{-/-}$Bcl2^{tg} *mice*

Organs other than the lungs were examined next. In young *Runx1*$^{-/-}$*Bcl2*^{tg} mice, tissues from the kidneys, liver, pancreas, or the digestive tract exhibited normal histology (data not shown). In contrast, aged *Runx1*$^{-/-}$*Bcl2*^{tg} mice developed a wasting disease of various organs, including muscles. For example, in the liver of aged mice (Fig. 4A), hepatocytes were atrophic, whereas sinusoids were enlarged and contained immune cells. Glycogenesis appeared insufficient, probably due to ischemia. The hemocyte count of peripheral blood (Table I) revealed slightly increased numbers of RBC and increased hemoglobin concentration and hematocrit percentage, suggesting compensatory erythrocytosis, whereas the numbers of WBC were decreased to less than half. In addition, the percentages of Gr-1^{med}Mac-1$^+$ monocytes were remarkably increased in peripheral blood (monocytosis in Fig. 4B), suggesting the presence of a chronic systemic inflammation in aged *Runx1*$^{-/-}$*Bcl2*^{tg} mice. Consistently, the levels of IFN-γ and TNF were elevated in sera from aged *Runx1*$^{-/-}$*Bcl2*^{tg} mice compared with control mice (Fig. 4C).

Altogether, the phenotypes described above suggest that active inflammation, such as lymphocyte infiltration, was initially limited to local areas in the lung of young *Runx1*$^{-/-}$*Bcl2*^{tg} mice. Subsequently, chronic and exacerbated immune responses resulted in SIRS in the aged *Runx1*$^{-/-}$*Bcl2*^{tg} mice, as exemplified by symptoms such as wasting disease, organ dysfunction, and lethality. In addition, aged *Runx1*$^{-/-}$*Bcl2*^{tg} mice developed a pathology similar to PAP.

Runx1-deleted CD4$^+$ T cells traffic to the lung and initiate lung inflammation

To examine whether the lung-infiltrating cells in *Runx1*$^{-/-}$*Bcl2*^{tg} mice were Runx1-deleted CD4$^+$ T cells, immunofluorescent de-

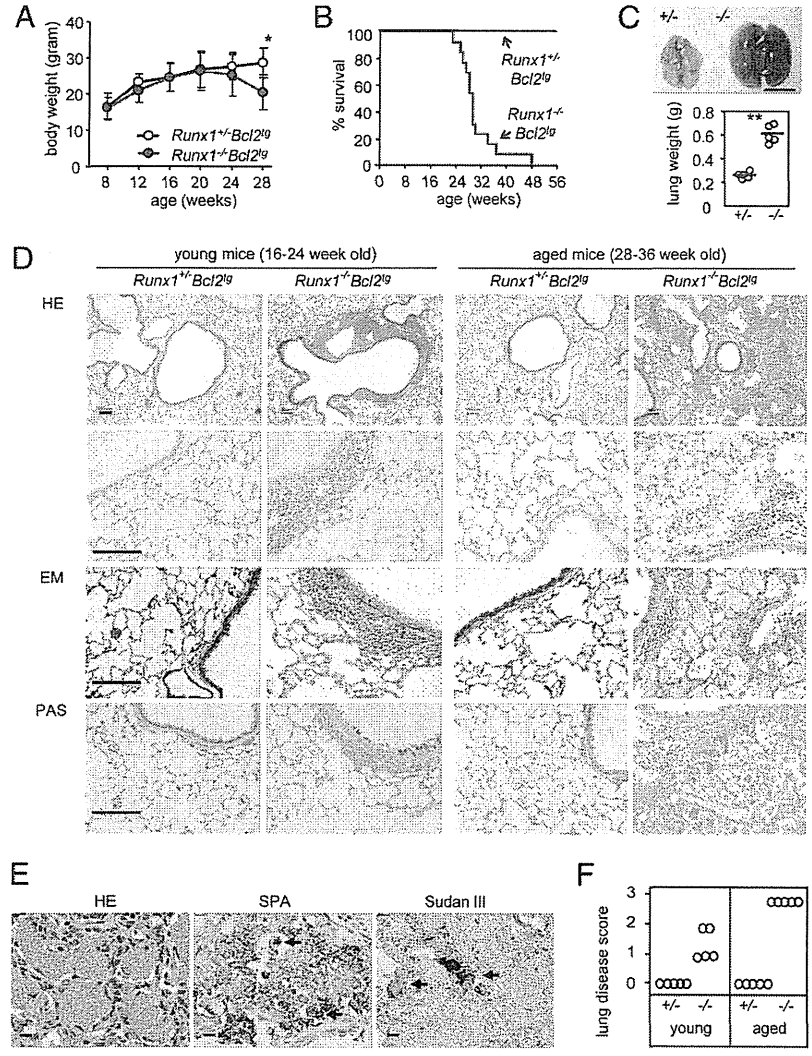

FIGURE 2. Mice harboring *Runx1*-deficient T cells develop lethal lung inflammation. **(A)** Weight loss in aged $Runx1^{-/-}Bcl2^{tg}$ mice. Body weights of $Runx1^{-/-}Bcl2^{tg}$ and control mice between 8 and 28 wk of age. Shown are mean ± SD (n = 6–8 mice per each age group). *p = 0.0038. **(B)** Reduced survival of $Runx1^{-/-}Bcl2^{tg}$ mice. Survival rate percentages of control and $Runx1^{-/-}Bcl2^{tg}$ mice within 1 y of age (n = 13). **(C)** A representative photograph of lungs derived from >28-wk-old control ($^{+/-}$) or $Runx1^{-/-}Bcl2^{tg}$ ($^{-/-}$) mice (*top panel*). The lungs from $Runx1^{-/-}Bcl2^{tg}$ mice became enlarged and diffusively red. Weights of lungs from >28-wk-old control ($^{+/-}$) and $Runx1^{-/-}Bcl2^{tg}$ ($^{-/-}$) mice (n = 5–6; *bottom panel*). **p = 0.000003. **(D)** Histology of lung tissue sections of control and $Runx1^{-/-}Bcl2^{tg}$ mice. Tissues were stained with H&E, EM, or PAS (n = 5). Scale bars, 100 μm. **(E)** PAP-like histology in the lungs of aged $Runx1^{-/-}Bcl2^{tg}$ mice. Lung sections were stained with H&E or Sudan III or counterstained with an Ab to surfactant protein A (SPA). n = 3. Scale bars, 10 μm. **(F)** Lung disease scores of control ($^{+/-}$) and $Runx1^{-/-}Bcl2^{tg}$ ($^{-/-}$) mice at the indicated ages (n = 5).

tection of the CD4 Ag was performed in frozen lung sections (Fig. 5A). As expected, $CD4^+$ T cells concentrated in the peribronchovascular regions of $Runx1^{-/-}Bcl2^{tg}$ (but not control) lungs.

The mechanism by which the Runx1-deleted $CD4^+$ T cells preferentially targeted the lungs was investigated by assessing whether Runx1 deletion caused deregulation of the expression of integrins. $CD4^+$-gated fractions from $Runx1^{-/-}Bcl2^{tg}$ splenocytes showed reduced expression of CD62L, a marker of homing to lymphoid organs (Fig. 5B). Expression of the gastrointestinal homing markers CD103 and CCR9 was subtle in $Runx1^{-/-}Bcl2^{tg}$ cells; in contrast, CD11a expression was substantially enhanced. Runx1 was reported to regulate CD11a expression by binding to a Runx site in the promoter (30). CD11a is a subunit of LFA-1, which interacts with ICAM1 expressed on the vessel wall in bronchial mucosa (31). We also examined chemokine receptors, such as CXCR3 and CCR5, which are important for lung infiltration (32, 33). Interestingly, the cell surface level of CXCR3 was increased, whereas CCR5 was not markedly changed in $Runx1^{-/-}Bcl2^{tg}$ $CD4^+$ T cells. Therefore, increased expression of CD11a and CXCR3 might cause the retention of Runx1-deficient $CD4^+$ cells in the lung.

The detection of various types of immune cells in the aged $Runx1^{-/-}Bcl2^{tg}$ lungs suggested that the infiltrating Runx1-deleted $CD4^+$ T cells may be responsible for the subsequent inflammation in the lungs. To address this possibility, $Runx1^{-/-}Bcl2^{tg}$ $CD4^+$ T cells were adoptively and intravenously transferred into $CD4^+$ T cell-deficient mice, and the lungs of these recipient mice were examined. Interestingly, recipient mice injected with $Runx1^{-/-}Bcl2^{tg}$ $CD4^+$ T cells showed lung phenotypes similar to those of donor mice, and disease scores were 1–2 at 5 wk and 2–3 at 25 wk postinjection (Fig. 5C, 5D). Infiltration of lymphocytes to the peribronchovascular region of recipient mice lungs strongly suggested that the Runx1-deleted $CD4^+$ T cells were capable of homing to the lungs, activating an immune response and causing inflammation.

Runx1-deleted $CD4^+$ T cells are hyperactivated

To better understand the mechanisms underlying the aggressive immune responses of $Runx1^{-/-}Bcl2^{tg}$ mice, spleens, pLN, and mLN were excised from nonimmunized control mice and $Runx1^{-/-}Bcl2^{tg}$ mice and examined by flow cytometry (Fig. 6A). As seen in the summary of Fig. 6B, naive cells ($CD44^{lo}CD62L^{hi}$) constituted only a small proportion (13 ± 9.3%) of the $CD4^+$-gated population in $Runx1^{-/-}Bcl2^{tg}$ lymphatic tissues compared with control tissues (49 ± 14%). Meanwhile, the majority of $CD4^+$-gated cells exhibited an active/memory phenotype ($CD44^{hi}$) in $Runx1^{-/-}Bcl2^{tg}$ tissues compared with control tissues (76 ± 13% versus 41 ± 10%). In addition, a 1.5–2.0-fold increase in the $CD69^+$ and $CD40L^+$ fractions was observed in the $CD4^+$-gated

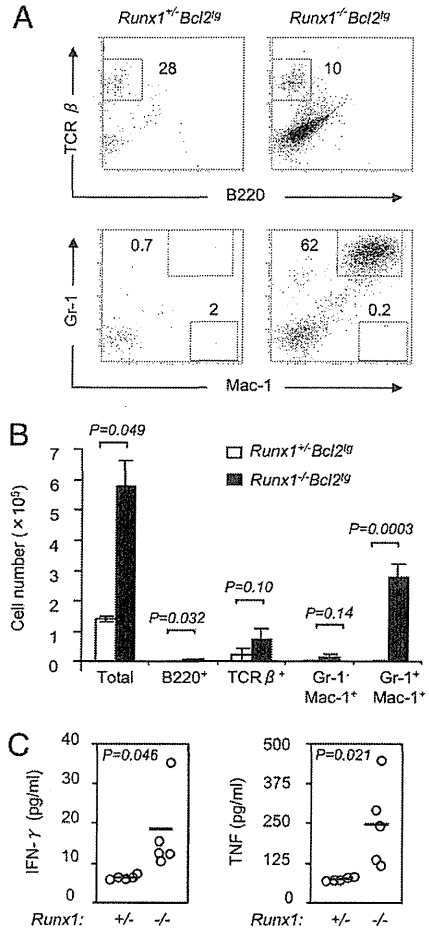

FIGURE 3. Increase in immune cells and proinflammatory cytokines in BALF of *Runx1*$^{-/-}$*Bcl2*^{tg} mice. (**A**) Flow cytometry analyses of cells in BALF. Representative results from three independent experiments are shown. (**B**) Bar graphs show mean (± SD) cell counts in BALF prepared from 24–32-wk-old control and *Runx1*$^{-/-}$*Bcl2*^{tg} mice (n = 3). Immune cells, including lymphocytes (B220$^+$ and TCRβ$^+$) and neutrophils (Gr-1$^+$Mac-1$^+$), were increased in *Runx1*$^{-/-}$*Bcl2*^{tg} mice. The B220$^+$ fraction constituted a small population in BALF but was increased in *Runx1*$^{-/-}$*Bcl2*^{tg} mice (1329 ± 1681 versus 7725 ± 106). (**C**) Amounts of proinflammatory cytokines IFN-γ and TNF in BALF derived from >28-wk-old control ($^{+/-}$) or *Runx1*$^{-/-}$*Bcl2*^{tg} ($^{-/-}$) mice (n = 5).

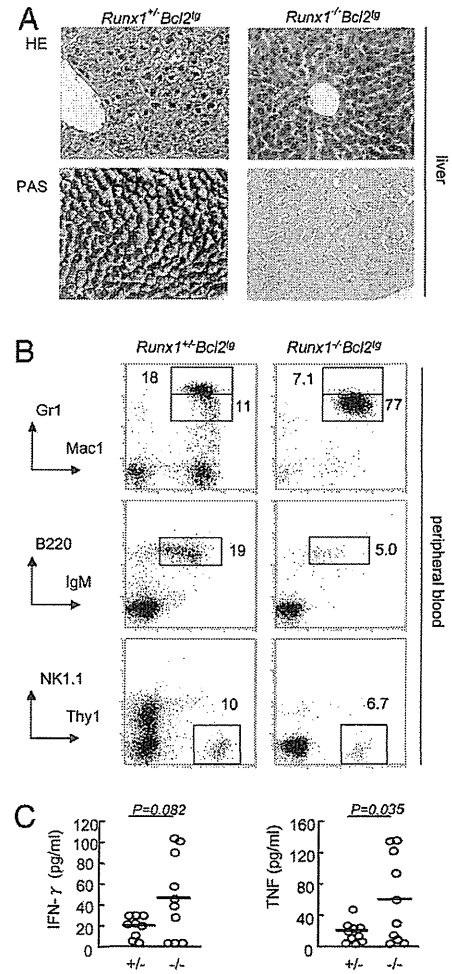

FIGURE 4. Aged *Runx1*$^{-/-}$*Bcl2*^{tg} mice develop SIRS. (**A**) Glycogenesis insufficiency in livers of aged *Runx1*$^{-/-}$*Bcl2*^{tg} mice. Liver sections from 28–36-wk-old control and *Runx1*$^{-/-}$*Bcl2*^{tg} mice were stained. H&E staining showed atrophy of hepatocytes, as well as enlargement of sinusiods. PAS-positive materials were abundant in the periphery of hepatocytes of control mice but were not detected in the *Runx1*$^{-/-}$*Bcl2*^{tg} hepatocytes, suggesting poor glycogenesis. Original magnification ×40. (**B**) Monocytosis in aged *Runx1*$^{-/-}$*Bcl2*^{tg} mice. Peripheral blood was collected from aged (>28-wk-old) control and *Runx1*$^{-/-}$*Bcl2*^{tg} mice and analyzed by flow cytometry staining. The percentage of monocytes (Gr-1^{int}Mac-1^{hi}) was dramatically increased in *Runx1*$^{-/-}$*Bcl2*^{tg} mice, indicating a presence of chronic inflammation and suggesting an increased demand for, for example, phagocytotic activity in the inflamed tissues. Percentages of other lineages, including B (B220$^+$IgM$^+$), NK (NK1.1$^+$), or T (Thy1$^+$) cells, were relatively reduced as the result of an increase in monocytes. Data are representative of two independent experiments. Note that monocytosis was not observed in the peripheral blood of young *Runx1*$^{-/-}$*Bcl2*^{tg} mice. (**C**) Elevated levels of proinflammatory cytokines in sera from aged *Runx1*$^{-/-}$*Bcl2*^{tg} mice. Sera were collected from aged (>28-wk-old) control ($^{+/-}$) and *Runx1*$^{-/-}$*Bcl2*^{tg} ($^{-/-}$) mice (n = 10 for each genotype). Amounts of IFN-γ (*left panel*) and TNF (*right panel*) were measured by cytokine bead array, using 5-fold diluted sera. The p values were evaluated by the unpaired Student t test.

Runx1$^{-/-}$*Bcl2*^{tg} tissues compared with control tissues (Fig. 6C, 6D). These findings indicated the continuous activation of Runx1-deleted CD4$^+$ T cells.

One possible explanation for the presence of autoactivated T cells is the escape of immature, self-reactive thymocytes into the periphery. Examination of thymocyte differentiation (Supplemental Fig. 1) revealed that the percentage of CD4-single positive cells was reduced to half in *Runx1*$^{-/-}$*Bcl2*^{tg} mice (2.4% compared with 4.4% in the control). However, the percentage of HSA^{low} TCR-β$^+$ mature cells in the CD4$^+$ gate did not differ significantly between control and *Runx1*$^{-/-}$*Bcl2*^{tg} thymuses (37% versus 33%). Furthermore, most of the CD4$^+$ cells in the two spleen genotypes belonged to a mature stage (89% versus 88%). Therefore, despite the delay in early thymocyte development in *Runx1*$^{-/-}$*Bcl2*^{tg} mice, CD4$^+$ cells appeared to be released into the periphery as fully mature T cells.

Another explanation for the presence of autoactivated CD4$^+$ T cells could be the expansion of a particular T cell clone capable of recognizing a specific Ag. To address this possibility, the expression of TCR V region β-chains (Vβ) in control and *Runx1*$^{-/-}$*Bcl2*^{tg} CD4$^+$ T cells was analyzed (Supplemental Fig. 2). Similar distribution patterns of TCR Vβ were observed in the two cell genotypes, confirming the polyclonality of cells.

A third possible explanation for autoactivated T cells is the dysfunction of Treg. As seen in Supplemental Fig. 3A, the percentage of Foxp3$^+$ cells among the CD4$^+$ subset was increased in *Runx1*$^{-/-}$*Bcl2*^{tg} spleens compared with control spleens (37%

Table I. Hemocyte counts

	Runx1$^{+/-}$ *Bcl2*^{tg}		*Runx1*$^{-/-}$ *Bcl2*^{tg}	
	Young	Aged	Young	Aged
WBC ($\times 10^2/\mu l$)	233 ± 90	223 ± 43	230 ± 54	94 ± 70
RBC ($\times 10^4/\mu l$)	993 ± 84	985 ± 28	993 ± 54	1150 ± 171
HGB (g/dl)	15 ± 1	15 ± 1	15 ± 1	16 ± 2
HCT (%)	48 ± 4	48 ± 1	48 ± 3	51 ± 6
MCV (fl)	48 ± 1	49 ± 1	48 ± 2	45 ± 3
MCH (pg)	15 ± 0	15 ± 1	15 ± 1	14 ± 1
MCHC (g/dl)	31 ± 1	32 ± 1	31 ± 1	32 ± 1
PLT ($\times 10^4/\mu l$)	97 ± 25	95 ± 4	90 ± 15	107 ± 40

Peripheral blood cell numbers from young (16–24-wk-old) and aged (>28-wk-old) control and *Runx1*$^{-/-}$*Bcl2*^{tg} mice were counted using Celltac-α machine (NihonKoden, Tokyo, Japan). Aged *Runx1*$^{-/-}$*Bcl2*^{tg} mice showed decreased numbers of WBC and increased numbers/values for RBC, hemoglobin (HGB), and hematocrit (HCT). Decreased WBC appears in accordance with the occurrence of SIRS in aged *Runx1*$^{-/-}$*Bcl2*^{tg} mice. In contrast, erythrocytosis suggests that the host's compensatory response mechanisms to a decreased oxygen supply to organs (hypoxia) is caused by severe lung inflammation and respiratory failure in aged *Runx1*$^{-/-}$*Bcl2*^{tg} mice. MCV, Mean corpuscular volume; MCH, mean corpuscular hemoglobin; MCHC, mean corpuscular hemoglobin concentration; PLT, platelet.

versus 14%). In support of this observation, increased *CTLA4* and *CD25* mRNA expression was detected in CD4$^+$ T cells purified from *Runx1*$^{-/-}$*Bcl2*^{tg} spleens (Supplemental Fig. 3B). An increase in Foxp3$^+$ Treg might function to circumvent the robust immune responses in *Runx1*$^{-/-}$*Bcl2*^{tg} mice. Therefore, the autoactivation of CD4$^+$ T cells seen in *Runx1*$^{-/-}$*Bcl2*^{tg} mice likely was not due to an impairment of thymocytes or Treg differentiation but rather was due to the dysregulation of intrinsic transcriptional control.

To further confirm an intrinsic process of CD4$^+$ T cell activation, we performed chimera experiments by transplanting BM cells from CD45.1$^+$-C57BL/6 and *Runx1*$^{-/-}$*Bcl2*^{tg} (CD45.1$^-$) mice into irradiated C57BL/6 recipient mice. Reconstituted cells in spleen, pLN, mLN, and lung of recipient mice were examined after 8 wk (Fig. 6E). CD4$^+$ T cells derived from *Runx1*$^{-/-}$*Bcl2*^{tg} BM contained a substantially greater percentage of memory/effector cells and fewer naive cells compared with the corresponding cells derived from wild-type BM. Notably, CD4$^+$ T cells from *Runx1*$^{-/-}$*Bcl2*^{tg} lung contained the highest percentage of effector/memory cells (84 ± 2%). The observations strongly suggest that Runx1 deficiency-mediated hyperactivation of CD4$^+$ T cells reflects a cell-intrinsic process.

Runx1-deleted CD4$^+$ T cells produce elevated levels of cytokines

To examine whether the Runx1-deleted CD4$^+$ T cells that showed an activated phenotype produced cytokines, the mRNA levels of cytokines were measured by RT-PCR (Fig. 7A). In the *Runx1*$^{-/-}$*Bcl2*^{tg} CD4$^+$ splenocytes, *IL-21* mRNA levels were 5-fold higher than in control cells (2.0 ± 0.09 versus 0.41 ± 0.24 folds). Similarly, the levels of proinflammatory cytokine *IL-17A* mRNA were also increased (1.9 ± 0.18 versus 0.29 ± 0.11). Consistent with our previous study (19), Runx1 deletion caused increased expression of the T cell growth factor cytokine *IL-2* (2.4 ± 0.68 versus 0.31 ± 0.38), which suggested actively dividing Runx1-deleted CD4$^+$ T cells. Furthermore, *IL-10* expression levels were increased (2.1 ± 0.45 versus 0.08 ± 0.05), which was in accordance with the increased percentage of Treg in *Runx1*$^{-/-}$*Bcl2*^{tg} mice. These data suggested that the Runx1 deletion in naive CD4$^+$ T cells led to spontaneous hyperactivation of cells, as reflected in the transcriptional induction of a wide range of cytokines. No significant increase in the *IFN-γ* mRNA level was detected in *Runx1*$^{-/-}$*Bcl2*^{tg} cells.

The expression of cytokines was next examined by flow cytometry after in vitro stimulation of CD4$^+$ T cells with PMA plus

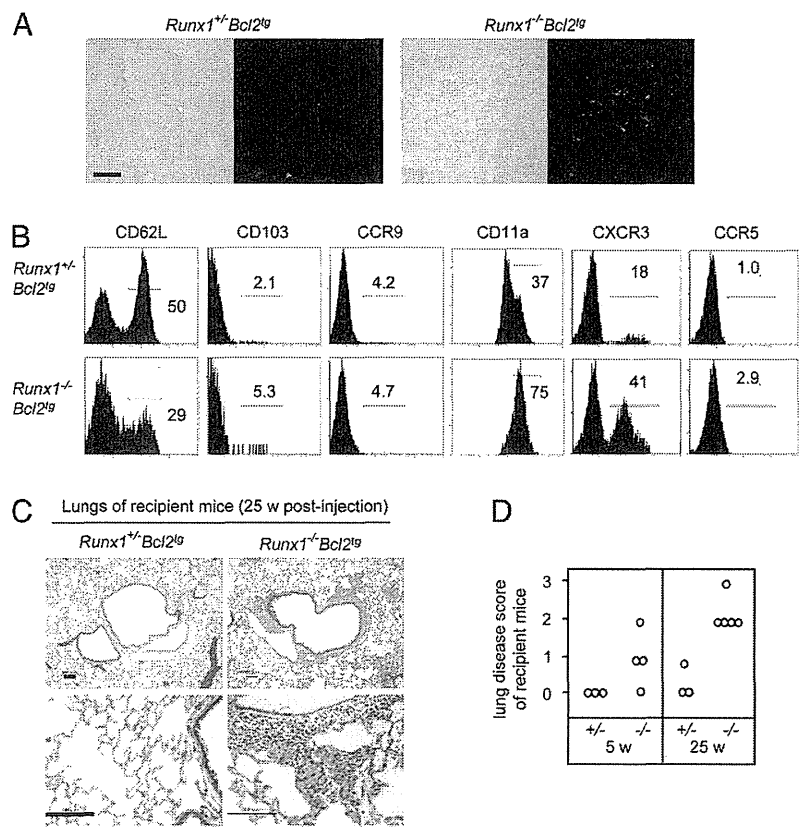

FIGURE 5. *Runx1*-deficient CD4$^+$ T cells infiltrate into the lung and initiate lung inflammation. (**A**) Accumulation of CD4$^+$ T cells in the lung interstitial region. Immunofluorescence staining of lung sections from >28-wk-old control and *Runx1*$^{-/-}$*Bcl2*^{tg} mice with an FITC-CD4 Ab. Scale bar, 100 μm. Data are representative of three independent experiments (n = 3). (**B**) Expression profiles of integrins and chemokine receptors in *Runx1*-deficient CD4$^+$ T cells. Surface expression of CD62L, CD103, CCR9, CD11a, CXCR3, and CCR5 in CD4$^+$ T-gated cells from control or *Runx1*$^{-/-}$*Bcl2*^{tg} spleens. Data are representative of three independent experiments. (**C** and **D**) Adoptive-transfer experiments of *Runx1*-deficient CD4$^+$ T cells. Control or *Runx1*$^{-/-}$*Bcl2*^{tg} CD4$^+$ T cells were isolated and injected into CD4$^+$ T cell-deficient mice. At 5 or 25 wk postinjection, recipient mice were sacrificed for lung examination. (C) Representative histology of lung sections from recipient mice at 25 wk postinjection. Sections were stained with H&E; scale bars, 100 μm. (D) Scoring of lung disease (n = 3–5).

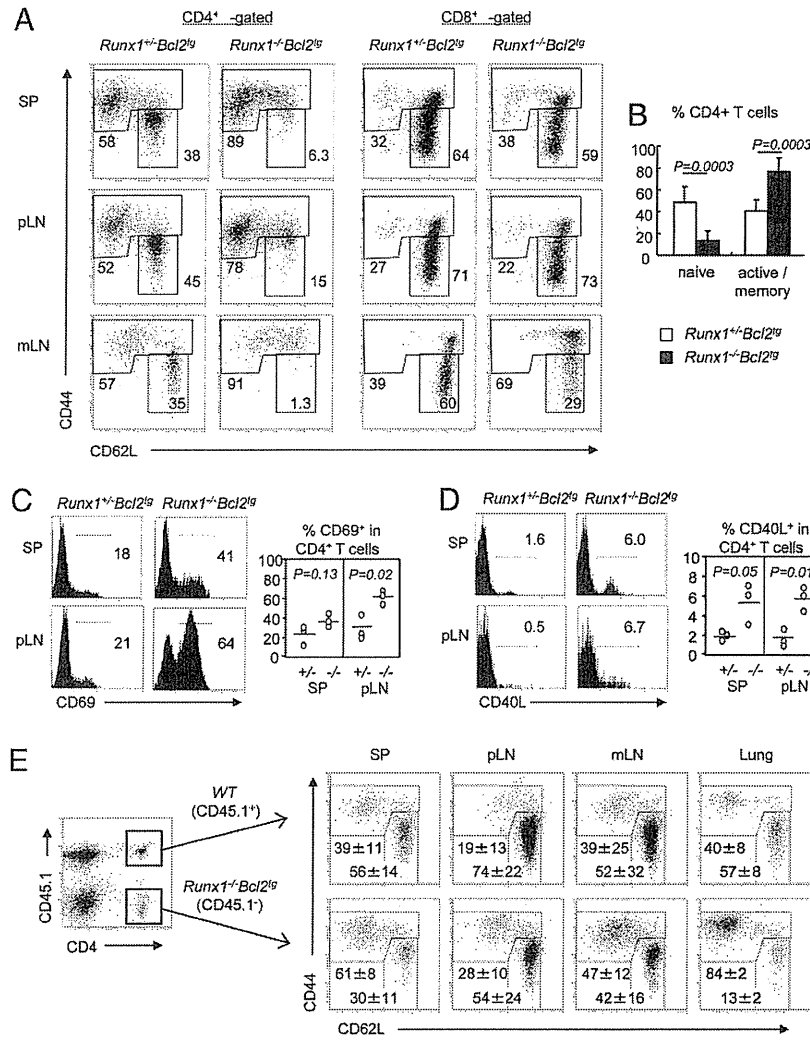

FIGURE 6. *Runx1*-deficient CD4$^+$ T cells are hyperactivated. (**A**) *Runx1*-deleted CD4$^+$ T cells gained active/memory phenotypes. Flow cytometry analyses of CD44 and CD62L expression on CD4$^+$ or CD8$^+$ T cells derived from spleens (SP), pLN, and mLN of 24–32-wk-old control and *Runx1*$^{-/-}$*Bcl2*^{tg} mice. The percentages of naive (CD62L^{hi}CD44^{lo}) and active/memory (CD62L^{lo} CD44^{hi} or CD62L^{hi}CD44^{hi}) fractions among the CD4$^+$- or CD8$^+$ T-gated cells are indicated. Data are representative of four independent experiments. (**B**) Bar graphs show the percentages (mean ± SD) of naive and active/memory cells among the CD4$^+$ fractions from control or *Runx1*$^{-/-}$*Bcl2*^{tg} mice. The average percentage was calculated from SP, pLN, and mLN (n = 4). (**C** and **D**) Surface expression of the activation markers CD69 and CD40L in CD4$^+$ T cells from spleens and pLN of 24–32-wk-old control or *Runx1*$^{-/-}$*Bcl2*^{tg} mice. Data are representative of three independent experiments (n = 3). (**E**) Flow cytometry analyses of naive versus active/memory phenotypes in CD4$^+$ T cells reconstituted by mixed-BM chimera experiment. C57BL/6 mice were lethally irradiated and transplanted by a mixture of wild-type (WT; CD45.1$^+$) and *Runx1*$^{-/-}$*Bcl2*^{tg} (CD45.1$^-$) BM cells. After 8 wk, spleen (SP), pLN, mLN, and lung were prepared and analyzed. Numbers shown are mean ± SD from two independent experiments (n = 4).

ionomycin (Fig. 7B). The percentages of IL-21$^+$ and IL-17$^+$ cells were several-fold higher in the spleens and pLN of *Runx1*$^{-/-}$*Bcl2*^{tg} mice compared with controls, suggesting that the *Runx1*$^{-/-}$*Bcl2*^{tg} CD4$^+$ T cells were more or less committed to differentiate into cytokine-producing effector T cells.

Runx1 suppresses the transcription of IL-21

Runx1 is reported to regulate the transcription of *IL-2*, *IL-4*, and *IL-17* (12, 13, 19). The role of Runx1 in *IL-21* expression is not known, although the role of IL-21 in both inflammation and the formation of IgG-secreting plasma cells is well established. This prompted an examination of the transcriptional regulation of IL-21 by Runx1. Transcription of *IL-21* is controlled by two DNase-hypersensitive sites (HS) designated promoter (P)/HS1 and HS2 (34). Using Vista comparative genomic tools, an additional CNS was identified in intron 2 (Fig. 8A). This ~500-bp region of CNS was 99% identical between human and mouse, suggesting that it has a potentially important function. The P, HS2, and CNS sequences from different species were aligned and searched for Runx binding sites. Notably, two Runx binding sites were identified in the CNS region (Supplemental Fig. 4) but not in the P or HS2 regions. To test the functional significance of the CNS region, the P and CNS regions of *IL-21* were ligated to a luciferase reporter (Fig. 8B). When transfected into Jurkat cells, both P-Luc and CNS+P-Luc plasmids showed only minimal basal activity. However, PMA plus ionomycin treatment of cells markedly induced P activity (27 ± 3-fold), as previously reported (34, 35). The addition of the CNS region further enhanced the reporter activity (42 ± 4-fold), indicating positive regulation by a response element in the CNS.

To examine whether Runx1 is involved in the regulation of CNS activity, the reporters were cotransfected with a Runx1-expressing vector, which was induced by PMA plus ionomycin (Fig. 8C). Runx1 reduced CNS+P-Luc activity to 50%, whereas it did not affect P-Luc activity. As a control, the cotransfection of Runt, a dominant-negative form of Runx1, did not reduce the CNS+P-Luc activity. In the case of CNS+SV40P-Luc, in which the *IL-21* promoter was replaced by the SV40 promoter, Runx1 reduced the activity to 30%, confirming the negative role of the CNS region in *IL-21* regulation (Fig. 8D). Mutations were then introduced into two Runx sites in the CNS, individually or simultaneously (Fig. 8E). Mutations of the Runx site at +3114 (m1), +3162 (m2), or both sites (m1&m2) partially or completely abolished the Runx1-mediated reduction in CNS activity.

ChIP assay was carried out to examine Runx1 binding to the *IL-21* CNS region. Lysates prepared from unstimulated CD4$^+$ T cells from C57BL/6 mice were immunoprecipitated with a Runx1 Ab. Sequences spanning each Runx site in the CNS, but not the promoter, were recovered as enriched (Fig. 8F). To further confirm the Runx1 binding, a concentrated DNA library was prepared and processed for quantitative real-time PCR. The CNS-1 and CNS-2 regions were successfully enriched (Fig. 8G). The results collec-

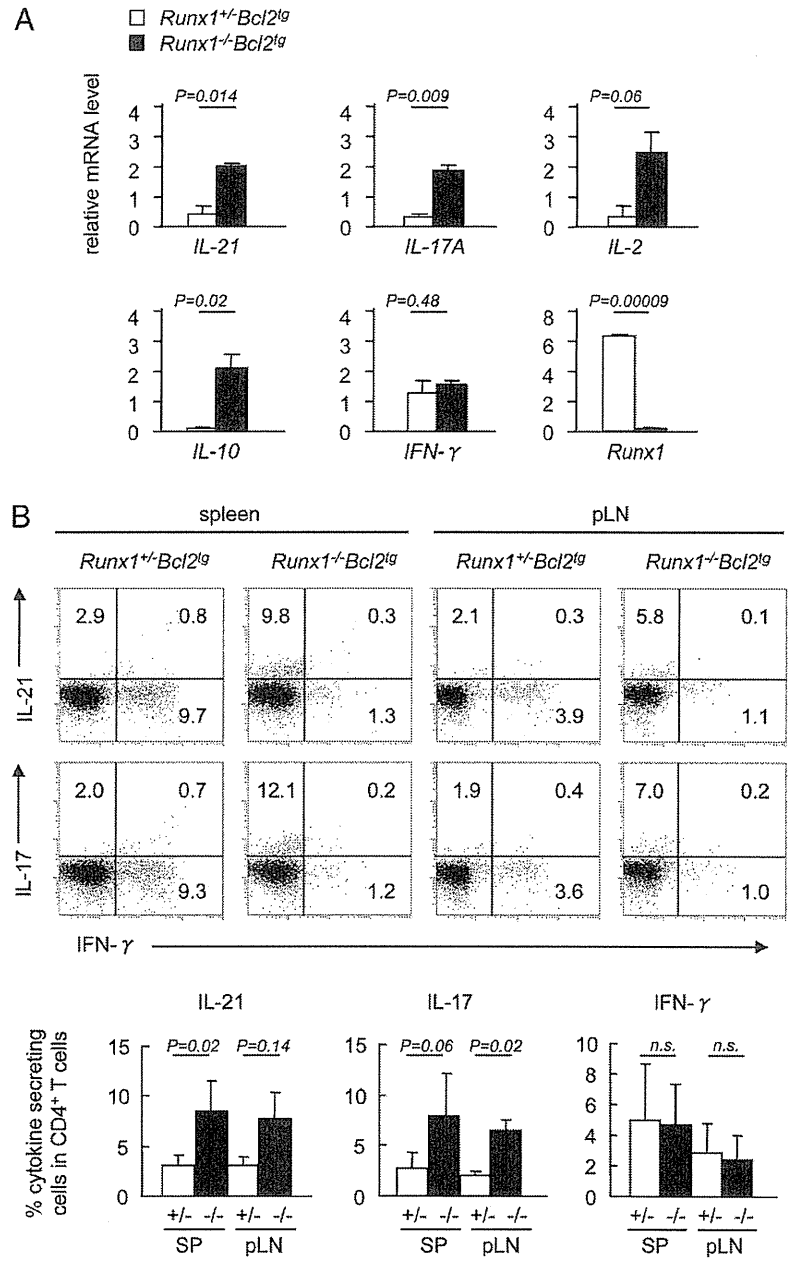

FIGURE 7. Enhanced expression of IL in *Runx1*-deficient $CD4^+$ T cells. (**A**) Relative amounts of *IL* transcripts compared with those of *β-actin*. $CD4^+$ T cells were purified from 24–32-wk-old control and $Runx1^{-/-}Bcl2^{tg}$ spleens. RNA was prepared and processed for semiquantitative RT-PCR analyses. Band intensities were compared and quantified, using *β-actin* as a control. Bar graphs are mean ± SD from two independent experiments. (**B**) $CD4^+$ T cells were purified from the spleens or pLN of 24–32-wk-old control and $Runx1^{-/-}Bcl2^{tg}$ mice. Cells were stimulated in vitro with PMA plus ionomycin and processed for intracellular staining of indicated IL and flow cytometry analyses. Representative data from three independent experiments are shown. Bar graphs show the percentages of cytokine-positive $CD4^+$ T cells in spleen or pLN from the control ($^{+/-}$) and $Runx1^{-/-}Bcl2^{tg}$ ($^{-/-}$) mice. Mean ± SD from three independent experiments is shown.

tively indicated that Runx1, if present, functions negatively to repress *IL-21* expression through binding to the CNS region.

Germinal center formation and Ab secretion in $Runx1^{-/-}Bcl2^{tg}$ *mice*

Increased expression of IL-21 was observed in Runx1-deleted $CD4^+$ T cells. An increase in IL-21 expression is associated with the development of inflammatory and autoimmune diseases in mice (36). For example, IL-21 can induce the differentiation of activated $CD4^+$ T cells into proinflammatory Th17 cells (37–39). In addition, IL-21 is important in promoting the formation of the germinal center (GC) and in the differentiation of B cells into Ig-secreting plasma cells (40–43).

Immunofluorescence was used to examine the effect of Runx1 deletion on GC formation, and the results showed that T ($CD4^+$) and B ($B220^+$) cell zones in white pulps were disrupted in $Runx1^{-/-}Bcl2^{tg}$ spleens (Fig. 9A). Furthermore, in white pulps of $Runx1^{-/-}Bcl2^{tg}$ spleens, IgD^+ naive B cells were not detected in the follicle region; PNA (a GC marker)-positive cells were detected instead (Fig. 9B). Analysis by flow cytometry (Fig. 9C) revealed a 2-fold increase in PNA^+Fas^{hi} cells (both are GC markers) in the $Runx1^{-/-}Bcl2^{tg}$-derived $CD4^+$ fraction compared with the control (28 ± 10% versus 14 ± 6%), whereas a 1.5-fold increase in PNA^+Fas^{hi} cells was detected in the $Runx1^{-/-}Bcl2^{tg}$-derived $B220^+$ fractions (13 ± 9.6% versus 8.2 ± 4.1%). These observations indicate that GC formation is accelerated spontaneously in Runx1-deleted spleens.

Because GC formation is associated with the expansion of B cells and Ig class switching, B cell phenotypes were examined further. A 2-fold increase in syndecan-1^+B220^{med} Ig-secreting plasma cells was observed in $Runx1^{-/-}Bcl2^{tg}$ spleens compared with controls (3.7 ± 0.6% versus 1.8 ± 0.4%; Fig. 9D).

The possible development of hyperimmunoglobulinemia in $Runx1^{-/-}Bcl2^{tg}$ mice was examined by measuring titers of Ig isotypes in sera. IgM and IgG2a levels (but not IgG1) were moderately increased in $Runx1^{-/-}Bcl2^{tg}$ mice compared with

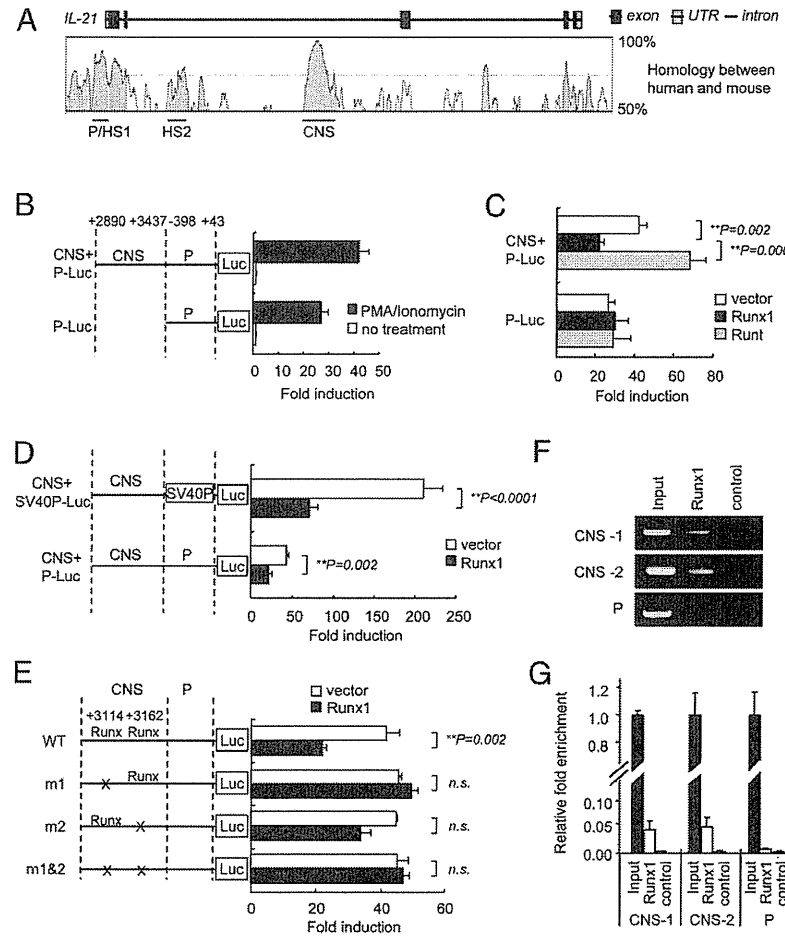

FIGURE 8. Runx1 controls *IL-21* transcription as revealed by reporter assays. (**A**) Homology of *IL-21* gene sequences between humans and mice, as detected by Vista browser. Location of the *IL-21* promoter (P), DNase-hypersensitive sites (HS1 or HS2), and CNS are indicated. (**B**) Jurkat cells were transfected with *IL-21* CNS+P-Luc or P-Luc reporters and treated or not with PMA plus ionomycin. (**C–E**) Jurkat cells were cotransfected with an *IL-21* reporter and an empty, Runx1- or Runt-expressing vector and stimulated with PMA plus ionomycin. (E) Mutations introduced into the Runx sites at +3114 or +3162 are indicated by "x." In (B)–(E), the reporter activities recovered are shown as fold induction (mean ± SD). In one experiment, samples were run in triplicate; representative results of three independent experiments are shown. (**F**) Runx1 binds to the *IL-21* CNS region inside cells. $CD4^+$ T cells from C57BL/6 mice were subjected to ChIP with anti-Runx1 Ab or control IgG, and the precipitates were processed for PCR. (**G**) Relative amounts of input, anti-Runx1 ChIP, or control in a concentrated library, as quantified by real-time PCR. In (F) and (G), the precipitated DNA was amplified with primers to CNS-1 (recognizing the Runx-site at +3114), CNS-2 (recognizing the Runx site at +3162), and negative control P (promoter harboring no Runx site). n.s., not significant.

control mice (Fig. 9E). Interestingly, the titers of anti-dsDNA Ab were also higher in *Runx1*$^{-/-}$*Bcl2*^{tg} mice than in control mice. However, the titer of anti-dsDNA in *Runx1*$^{-/-}$*Bcl2*^{tg} mice was a few-fold lower than in aged *MPL*$^{lpr/lpr}$ mice (data not shown). Finally, frozen sections of lung were stained by fluorescein-tagged anti-IgG (Fig. 9F). Some interstitial lymphoid cells were positive for IgG staining, an indication of plasma cells. Altogether, the above observations suggest that plasma cell-associated humoral responses, including autoantibodies, might be involved in lung pathogenesis.

Discussion

Runx1$^{-/-}$*Bcl2*^{tg} mice generated in this study developed severe lung disease in the absence of Ag challenge. Mixed pathological phenotypes were observed, such as lymphoid infiltration into peribronchovascular interstitial regions and granulocyte-, foamy macrophage-, and surfactant protein A-containing exudates into alveolar spaces. Also, high titers of proinflammatory cytokines in BALF suggested the existence of severe inflammatory responses in the lungs. Additionally, the mice suffered from systemic inflammatory responses and died at ~6–7 mo of age.

It is noteworthy that some of the pathology seen in *Runx1*$^{-/-}$*Bcl2*^{tg} lungs resembled PAP in humans. In 90% of cases of human PAP, the emergence of neutralizing autoantibodies against GM-CSF in sera appears to be responsible for the pathogenesis (44). In mouse models, PAP is generated by targeting GM-CSF, and mice exhibit pulmonary lymphoid hyperplasia, as well as alveolar proteinosis (45, 46). In humans and mice that lack GM-CSF signaling, the accumulation of exudates in alveolar spaces is attributed to a dysfunction of alveolar macrophages in clearing surfactant proteins (29). In our *Runx1*$^{-/-}$*Bcl2*^{tg} mice, anti–GM-CSF autoantibodies were not detected in sera (data not shown), and alveolar macrophages were found to be positive for surfactant protein A and Sudan III, an indication of cellular engulfing activity. Although there are no reports linking T lymphocyte abnormality to PAP, a possible cytokine storm in the lung might somehow cause macrophage dysfunction and the consequent failure to digest the incorporated materials.

It must be noted that although GM-CSF–null mice suffer from lung disease, the mice are apparently healthy and have a normal life span. In contrast, *Runx1*$^{-/-}$*Bcl2*^{tg} mice died before they reached 6–7 mo old, suggesting a much more severe and complicated pathogenesis in our mice. At a terminal stage in *Runx1*$^{-/-}$*Bcl2*^{tg} mice, systemic inflammation developed, probably due to the leakage of cytokines into the circulation. As signs of SIRS, various complications, such as monocytosis, blood coagulation, muscle wasting syndrome, and liver failure, commonly occur (10). Indeed, at least some of the above signs were confirmed in older *Runx1*$^{-/-}$*Bcl2*^{tg} mice. In addition, the chronic reactivity of $CD4^+$ T cells is reported to drive autoimmunity and destructive inflammation (47). Thus, the characteristic pathology of *Runx1*$^{-/-}$*Bcl2*^{tg} mice would be the development of lung-localized inflammation as well as systemic inflammation.

Circulating T lymphocytes, while preserving their ability to fight invading pathogens, are maintained in a quiescent stage and prevented from unnecessary autoactivation. In early studies, quiescence was considered a default stage of mature T cells before encountering a cognate Ag. Subsequently, increasing numbers of

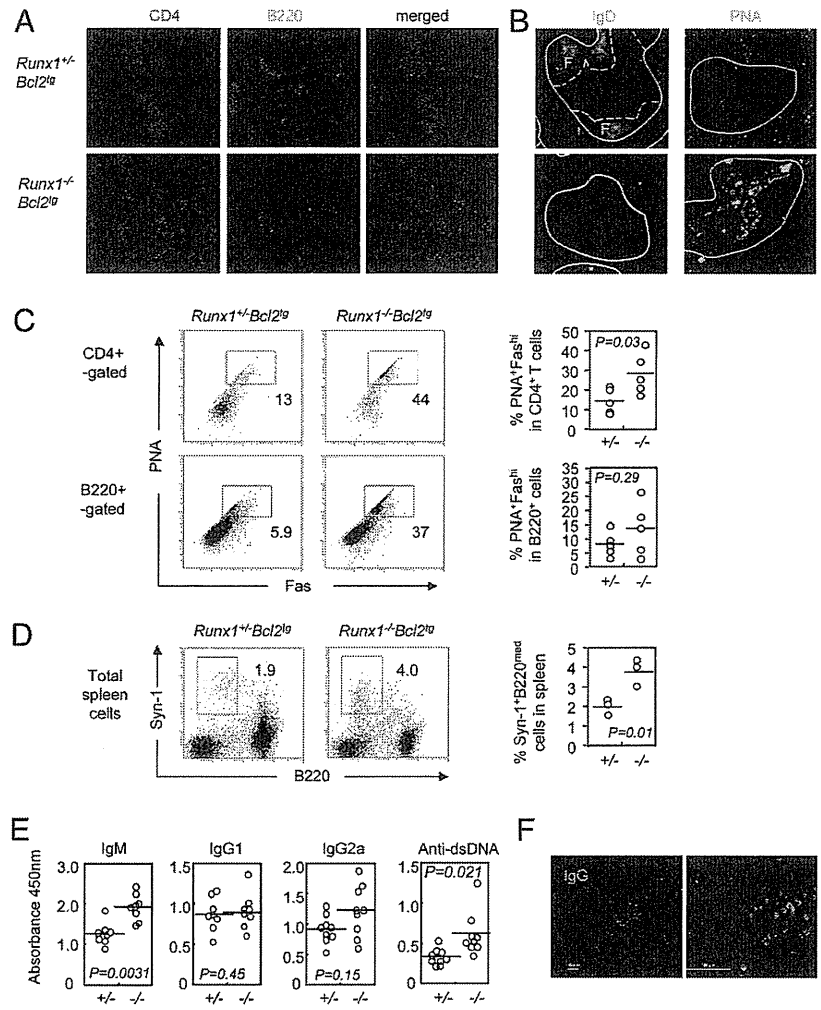

FIGURE 9. Enhancement of GC formation, plasma cell mobilization, and serum Ig levels in *Runx1*$^{-/-}$*Bcl2*^{tg} mice. (**A** and **B**) Immunofluorescence staining of spleens from 24–32-wk-old control and *Runx1*$^{-/-}$*Bcl2*^{tg} mice with anti-CD4, anti-B220, anti-IgD, or anti-PNA Abs. Representative images from two independent experiments are shown. White pulps and follicle areas (F) are indicated by solid and dashed white lines, respectively. Original magnification ×10. Flow cytometry analyses of PNA^{hi}Fas^{+} GC cells in CD4^{+} and B220^{+} splenocytes (**C**) and Syn-1^{hi}B220^{med} plasma B cells in splenocytes (**D**). Control ($^{+/-}$) and *Runx1*$^{-/-}$*Bcl2*^{tg} ($^{-/-}$) 24–32-wk-old mice were used. Data are representative of five (C) or three (D) independent experiments. (**E**) Levels of Ig subtypes in sera. ELISA analyses of IgM, IgG1, IgG2a, and anti-dsDNA in sera from 24–32-wk-old control ($^{+/-}$) and *Runx1*$^{-/-}$*Bcl2*^{tg} ($^{-/-}$) mice (n = 8–9). (**F**) Immunofluorescence staining of IgG on frozen lung sections from 24–32-wk-old *Runx1*$^{-/-}$*Bcl2*^{tg} mice. Scale bar, 100 μm. Data are representative of three independent experiments (n = 3).

studies suggested that the maintenance of quiescence in T cells required the activity of transcription factors, such as Klf2, Tob, Foxo, Slfn2, Tsc1, and Foxp1 (2–8). However, the thus-far reported quiescence-related molecules are also involved in the regulation of cell homeostasis, cell survival, and/or cell trafficking, and their targeting often results in a lymphopenic situation in mice. Therefore, the loss of cell quiescence seen in targeted mice might be due to the induction of cell proliferation to compensate for lymphopenia, and a quiescence control mechanism remains a controversial issue. We avoided this complexity by protecting cells from apoptosis with the use of the Bcl2 transgene and observed that *Runx1*$^{-/-}$*Bcl2*^{tg} CD4^{+} T cells exhibited hyperactivated phenotypes, as judged by the expression of activation markers (CD62L^{lo}CD44^{hi}CD69^{+}), the lung-homing integrin molecule CD11a, and various cytokines. The present results suggest that Runx1 may function as a guardian of naive CD4^{+} T cells in their quiescence stage.

Then how does a Runx1 deficiency lead to the disruption of cell quiescence? The spontaneous expression of various cytokines in naive *Runx1*$^{-/-}$*Bcl2*^{tg} CD4^{+} T cells suggests that Runx1 might contribute to quiescence by intrinsically suppressing the expression of various cytokines in resting T cells. Regulation of cytokine genes, such as *IL-2*, *IL-4*, or *IL-17*, by Runx1 was reported (12, 13, 19). In this study, we explored the regulation of *IL-21* transcription by Runx1 because IL-21 is closely associated with both inflammatory (37–39) and autoimmune diseases (41, 48). We found that the ectopic expression of Runx1 suppressed the PMA plus ionomycin-induced CNS activity of *IL-21*. Multiple Runx and NFAT binding sites were identified in the CNS region. One possibility is that Runx1 binding to the CNS suppresses *IL-21* transcription by masking the NFAT binding sites. Conversely, the lack of Runx1, as in the case of *Runx1*$^{-/-}$*Bcl2*^{tg} CD4^{+} T cells, is likely to cause an induction of *IL-21* transcription through a derepression mechanism.

IL-21 plays important roles in inflammation through its ability to induce IL-17 expression (37–39), whereas IL-17, in turn, mediates immunopathogenesis in experimental hypersensitivity pneumonitis and bronchiolitis obliterans syndrome [e.g. (49, 50)]. In a mouse model of experimental autoimmune encephalitis, IL-21 deficiency slowed disease progression as the result of a secondary effect of IL-17 reduction (38). In Runx1-deficient CD4^{+} T cells, expression of both IL-17 and IL-21 were increased. Augmentation of IL-21 might exacerbate lung inflammation indirectly through the enhancement of IL-17 expression in *Runx1*$^{-/-}$*Bcl2*^{tg} mice. However, an IL-17–independent role for IL-21, if any, in the inflammatory responses seen in *Runx1*$^{-/-}$*Bcl2*^{tg} lungs remains to be elucidated.

The known, direct effects of IL-21 are the enhancement of GC formation and the generation of IgG-secreting plasma cells (40–43). As seen in *Runx1*$^{-/-}$*Bcl2*^{tg} mice, an increased percentage of B cells became plasma cells in the spleen GC. IgG^{+} plasma cells were detected in the lung, although it is not clear whether they produced autoantibodies that contributed to pathogenesis in the *Runx1*$^{-/-}$*Bcl2*^{tg} lungs. Levels of IgM, IgG2a, and anti-dsDNA Ab

in sera were moderately increased, indicating the mobilization of humoral immune responses. It is possible that Abs produced by IgG^+ plasma cells might cooperate with other immune cells and exacerbate the localized immune responses in the lung, as well as systemic inflammation.

In conclusion, the current study suggests a novel role for the Runx1 transcription factor in maintaining the quiescent stage of mature $CD4^+$ T cells in peripheral lymphoid tissues. Deletion of Runx1 in naive $CD4^+$ T cells caused spontaneous cellular activation and cytokine production that eventually led to a catastrophic autoimmune inflammatory disease. The pathology seen in *Runx1*$^{-/-}$*Bcl2*^{tg} lungs was similar to that of human PAP. This study also implies a therapeutic potential of the Runx1 molecule for the suppression of inflammatory disease mediated by hyperactivated $CD4^+$ T cells.

Acknowledgments

We thank I. Taniuchi (RIKEN, Yokohama, Japan) for CD4-Cre-tg mice and Y. Yoshikai and H. Yamada (Kyushu University, Kyushu, Japan) for *Bcl2*^{tg} mice. We thank M. Kuji for secretarial assistance.

Disclosures

The authors have no financial conflicts of interest.

References

1. Yusuf, I., and D. A. Fruman. 2003. Regulation of quiescence in lymphocytes. *Trends Immunol.* 24: 380–386.
2. Berger, M., P. Krebs, K. Crozat, X. Li, B. A. Croker, O. M. Siggs, D. Popkin, X. Du, B. R. Lawson, and A. N. Theofilopoulos, et al. 2010. An Slfn2 mutation causes lymphoid and myeloid immunodeficiency due to loss of immune cell quiescence. *Nat. Immunol.* 11: 335–343.
3. Buckley, A. F., C. T. Kuo, and J. M. Leiden. 2001. Transcription factor LKLF is sufficient to program T cell quiescence via a c-Myc–dependent pathway. *Nat. Immunol.* 2: 698–704.
4. Feng, X., H. Wang, H. Takata, T. J. Day, J. Willen, and H. Hu. 2011. Transcription factor Foxp1 exerts essential cell-intrinsic regulation of the quiescence of naive T cells. *Nat. Immunol.* 12: 544–550.
5. Kuo, C. T., M. L. Veselits, and J. M. Leiden. 1997. LKLF: A transcriptional regulator of single-positive T cell quiescence and survival. *Science* 277: 1986–1990.
6. Medema, R. H., G. J. Kops, J. L. Bos, and B. M. Burgering. 2000. AFX-like Forkhead transcription factors mediate cell-cycle regulation by Ras and PKB through p27kip1. *Nature* 404: 782–787.
7. Tzachanis, D., G. J. Freeman, N. Hirano, A. A. van Puijenbroek, M. W. Delfs, A. Berezovskaya, L. M. Nadler, and V. A. Boussiotis. 2001. Tob is a negative regulator of activation that is expressed in anergic and quiescent T cells. *Nat. Immunol.* 2: 1174–1182.
8. Yang, K., G. Neale, D. R. Green, W. He, and H. Chi. 2011. The tumor suppressor Tsc1 enforces quiescence of naive T cells to promote immune homeostasis and function. *Nat. Immunol.* 12: 888–897.
9. Tzachanis, D., E. M. Lafuente, L. Li, and V. A. Boussiotis. 2004. Intrinsic and extrinsic regulation of T lymphocyte quiescence. *Leuk. Lymphoma* 45: 1959–1967.
10. Davies, M. G., and P. O. Hagen. 1997. Systemic inflammatory response syndrome. *Br. J. Surg.* 84: 920–935.
11. Wong, W. F., K. Kohu, T. Chiba, T. Sato, and M. Satake. 2011. Interplay of transcription factors in T-cell differentiation and function: the role of Runx. *Immunology* 132: 157–164.
12. Komine, O., K. Hayashi, W. Natsume, T. Watanabe, Y. Seki, N. Seki, R. Yagi, W. Sukzuki, H. Tamauchi, K. Hozumi, et al. 2003. The Runx1 transcription factor inhibits the differentiation of naive CD4+ T cells into the Th2 lineage by repressing GATA3 expression. *J. Exp. Med.* 198: 51–61.
13. Zhang, F., G. Meng, and W. Strober. 2008. Interactions among the transcription factors Runx1, RORgammat and Foxp3 regulate the differentiation of interleukin 17-producing T cells. *Nat. Immunol.* 9: 1297–1306.
14. Lazarevic, V., X. Chen, J. H. Shim, E. S. Hwang, E. Jang, A. N. Bolm, M. Oukka, V. K. Kuchroo, and L. H. Glimcher. 2011. T-bet represses T(H)17 differentiation by preventing Runx1-mediated activation of the gene encoding RORgammat. *Nat. Immunol.* 12: 96–104.
15. Ono, M., H. Yaguchi, N. Ohkura, I. Kitabayashi, Y. Nagamura, T. Nomura, Y. Miyachi, T. Tsukada, and S. Sakaguchi. 2007. Foxp3 controls regulatory T-cell function by interacting with AML1/Runx1. *Nature* 446: 685–689.
16. Zheng, Y., S. Josefowicz, A. Chaudhry, X. P. Peng, K. Forbush, and A. Y. Rudensky. 2010. Role of conserved non-coding DNA elements in the Foxp3 gene in regulatory T-cell fate. *Nature* 463: 808–812.
17. Kitoh, A., M. Ono, Y. Naoe, N. Ohkura, T. Yamaguchi, H. Yaguchi, I. Kitabayashi, T. Tsukada, T. Nomura, Y. Miyachi, et al. 2009. Indispensable role of the Runx1-Cbfbeta transcription complex for in vivo-suppressive function of FoxP3+ regulatory T cells. *Immunity* 31: 609–620.
18. Rudra, D., T. Egawa, M. M. Chong, P. Treuting, D. R. Littman, and A. Y. Rudensky. 2009. Runx-CBFbeta complexes control expression of the transcription factor Foxp3 in regulatory T cells. *Nat. Immunol.* 10: 1170–1177.
19. Wong, W. F., M. Kurokawa, M. Satake, and K. Kohu. 2011. Down-regulation of Runx1 expression by TCR signal involves an autoregulatory mechanism and contributes to IL-2 production. *J. Biol. Chem.* 286: 11110–11118.
20. Egawa, T., R. E. Tillman, Y. Naoe, I. Taniuchi, and D. R. Littman. 2007. The role of the Runx transcription factors in thymocyte differentiation and in homeostasis of naive T cells. *J. Exp. Med.* 204: 1945–1957.
21. Naoe, Y., R. Setoguchi, K. Akiyama, S. Muroi, M. Kuroda, F. Hatam, D. R. Littman, and I. Taniuchi. 2007. Repression of interleukin-4 in T helper type 1 cells by Runx/Cbf beta binding to the Il4 silencer. *J. Exp. Med.* 204: 1749–1755.
22. Ichikawa, M., T. Asai, T. Saito, S. Seo, I. Yamazaki, T. Yamagata, K. Mitani, S. Chiba, S. Ogawa, M. Kurokawa, and H. Hirai. 2004. AML-1 is required for megakaryocytic maturation and lymphocytic differentiation, but not for maintenance of hematopoietic stem cells in adult hematopoiesis. *Nat. Med.* 10: 299–304.
23. Lee, P. P., D. R. Fitzpatrick, C. Beard, H. K. Jessup, S. Lehar, K. W. Makar, M. Perez-Melgosa, M. T. Sweetser, M. S. Schlissel, S. Nguyen, et al. 2001. A critical role for Dnmt1 and DNA methylation in T cell development, function, and survival. *Immunity* 15: 763–774.
24. Strasser, A., A. W. Harris, and S. Cory. 1991. bcl-2 transgene inhibits T cell death and perturbs thymic self-censorship. *Cell* 67: 889–899.
25. Damayanti, T., T. Kikuchi, J. Zaini, H. Daito, M. Kanehira, K. Kohu, N. Ishii, M. Satake, K. Sugamura, and T. Nukiwa. 2010. Serial OX40 engagement on CD4+ T cells and natural killer T cells causes allergic airway inflammation. *Am. J. Respir. Crit. Care Med.* 181: 688–698.
26. Soroosh, P., S. Ine, K. Sugamura, and N. Ishii. 2006. OX40-OX40 ligand interaction through T cell-T cell contact contributes to CD4 T cell longevity. *J. Immunol.* 176: 5975–5987.
27. Kanto, S., N. Chiba, Y. Tanaka, S. Fujita, M. Endo, N. Kamada, K. Yoshikawa, A. Fukuzaki, S. Orikasa, T. Watanabe, and M. Satake. 2000. The PEBP2beta/CBF beta-SMMHC chimeric protein is localized both in the cell membrane and nuclear subfractions of leukemic cells carrying chromosomal inversion 16. *Leukemia* 14: 1253–1259.
28. Kohu, K., H. Ohmori, W. F. Wong, D. Onda, T. Wakoh, S. Kon, M. Yamashita, T. Nakayama, M. Kubo, and M. Satake. 2009. The Runx3 transcription factor augments Th1 and down-modulates Th2 phenotypes by interacting with and attenuating GATA3. *J. Immunol.* 183: 7817–7824.
29. Trapnell, B. C., J. A. Whitsett, and K. Nakata. 2003. Pulmonary alveolar proteinosis. *N. Engl. J. Med.* 349: 2527–2539.
30. Puig-Kröger, A., C. Lopez-Rodriguez, M. Relloso, T. Sanchez-Elsner, A. Nueda, E. Munoz, C. Bernabeu, and A. L. Corbi. 2000. Polyomavirus enhancer-binding protein 2/core binding factor/acute myeloid leukemia factors contribute to the cell type-specific activity of the CD11a integrin gene promoter. *J. Biol. Chem.* 275: 28507–28512.
31. Holt, P. G., D. H. Strickland, M. E. Wikstrom, and F. L. Jahnsen. 2008. Regulation of immunological homeostasis in the respiratory tract. *Nat. Rev. Immunol.* 8: 142–152.
32. Campbell, J. J., C. E. Brightling, F. A. Symon, S. Qin, K. E. Murphy, M. Hodge, D. P. Andrew, L. Wu, E. C. Butcher, and A. J. Wardlaw. 2001. Expression of chemokine receptors by lung T cells from normal and asthmatic subjects. *J. Immunol.* 166: 2842–2848.
33. Kohlmeier, J. E., T. Cookenham, S. C. Miller, A. D. Roberts, J. P. Christensen, A. R. Thomsen, and D. L. Woodland. 2009. CXCR3 directs antigen-specific effector CD4+ T cell migration to the lung during parainfluenza virus infection. *J. Immunol.* 183: 4378–4384.
34. Kim, H. P., L. L. Korn, A. M. Gamero, and W. J. Leonard. 2005. Calcium-dependent activation of interleukin-21 gene expression in T cells. *J. Biol. Chem.* 280: 25291–25297.
35. Mehta, D. S., A. L. Wurster, A. S. Weinmann, and M. J. Grusby. 2005. NFATc2 and T-bet contribute to T-helper-cell-subset-specific regulation of IL-21 expression. *Proc. Natl. Acad. Sci. USA* 102: 2016–2021.
36. Spolski, R., and W. J. Leonard. 2008. Interleukin-21: basic biology and implications for cancer and autoimmunity. *Annu. Rev. Immunol.* 26: 57–79.
37. Korn, T., E. Bettelli, W. Gao, A. Awasthi, A. Jager, T. B. Strom, M. Oukka, and V. K. Kuchroo. 2007. IL-21 initiates an alternative pathway to induce proinflammatory T(H)17 cells. *Nature* 448: 484–487.
38. Nurieva, R., X. O. Yang, G. Martinez, Y. Zhang, A. D. Panopoulos, L. Ma, K. Schluns, Q. Tian, S. S. Watowich, A. M. Jetten, and C. Dong. 2007. Essential autocrine regulation by IL-21 in the generation of inflammatory T cells. *Nature* 448: 480–483.
39. Zhou, L., I. I. Ivanov, R. Spolski, R. Min, K. Shenderov, T. Egawa, D. E. Levy, W. J. Leonard, and D. R. Littman. 2007. IL-6 programs T(H)-17 cell differentiation by promoting sequential engagement of the IL-21 and IL-23 pathways. *Nat. Immunol.* 8: 967–974.
40. Linterman, M. A., L. Beaton, D. Yu, R. R. Ramiscal, M. Srivastava, J. J. Hogan, N. K. Verma, M. J. Smyth, R. J. Rigby, and C. G. Vinuesa. 2010. IL-21 acts directly on B cells to regulate Bcl-6 expression and germinal center responses. *J. Exp. Med.* 207: 353–363.
41. Ozaki, K., R. Spolski, R. Ettinger, H. P. Kim, G. Wang, C. F. Qi, P. Hwu, D. J. Shaffer, S. Akilesh, D. C. Roopenian, et al. 2004. Regulation of B cell differentiation and plasma cell generation by IL-21, a novel inducer of Blimp-1 and Bcl-6. *J. Immunol.* 173: 5361–5371.

42. Ozaki, K., R. Spolski, C. G. Feng, C. F. Qi, J. Cheng, A. Sher, H. C. Morse III, C. Liu, P. L. Schwartzberg, and W. J. Leonard. 2002. A critical role for IL-21 in regulating immunoglobulin production. *Science* 298: 1630–1634.
43. Zotos, D., J. M. Coquet, Y. Zhang, A. Light, K. D'Costa, A. Kallies, L. M. Corcoran, D. I. Godfrey, K. M. Toellner, M. J. Smyth, et al. 2010. IL-21 regulates germinal center B cell differentiation and proliferation through a B cell-intrinsic mechanism. *J. Exp. Med.* 207: 365–378.
44. Kitamura, T., N. Tanaka, J. Watanabe, and S. Uchida Kanegasaki, Y. Yamada, and K. Nakata. 1999. Idiopathic pulmonary alveolar proteinosis as an autoimmune disease with neutralizing antibody against granulocyte/macrophage colony-stimulating factor. *J. Exp. Med.* 190: 875–880.
45. Dranoff, G., A. D. Crawford, M. Sadelain, B. Ream, A. Rashid, R. T. Bronson, G. R. Dickersin, C. J. Bachurski, E. L. Mark, J. A. Whitsett, et al. 1994. Involvement of granulocyte-macrophage colony-stimulating factor in pulmonary homeostasis. *Science* 264: 713–716.
46. Stanley, E., G. J. Lieschke, D. Grail, D. Metcalf, G. Hodgson, J. A. Gall, D. W. Maher, J. Cebon, V. Sinickas, and A. R. Dunn. 1994. Granulocyte/macrophage colony-stimulating factor-deficient mice show no major perturbation of hematopoiesis but develop a characteristic pulmonary pathology. *Proc. Natl. Acad. Sci. USA* 91: 5592–5596.
47. Palmer, M. T., and C. T. Weaver. 2010. Autoimmunity: increasing suspects in the CD4+ T cell lineup. *Nat. Immunol.* 11: 36–40.
48. Herber, D., T. P. Brown, S. Liang, D. A. Young, M. Collins, and K. Dunussi-Joannopoulos. 2007. IL-21 has a pathogenic role in a lupus-prone mouse model and its blockade with IL-21R.Fc reduces disease progression. *J. Immunol.* 178: 3822–3830.
49. Joshi, A. D., D. J. Fong, S. R. Oak, G. Trujillo, K. R. Flaherty, F. J. Martinez, and C. M. Hogaboam. 2009. Interleukin-17-mediated immunopathogenesis in experimental hypersensitivity pneumonitis. *Am. J. Respir. Crit. Care Med.* 179: 705–716.
50. Vanaudenaerde, B. M., S. I. De Vleeschauwer, R. Vos, I. Meyts, D. M. Bullens, V. Reynders, W. A. Wuyts, D. E. Van Raemdonck, L. J. Dupont, and G. M. Verleden. 2008. The role of the IL23/IL17 axis in bronchiolitis obliterans syndrome after lung transplantation. *Am. J. Transplant.* 8: 1911–1920.

Clin Exp Nephrol
DOI 10.1007/s10157-012-0684-5

REVIEW ARTICLE

Diagnosis and treatment of multiple myeloma and AL amyloidosis with focus on improvement of renal lesion

Kenshi Suzuki

Received: 28 May 2012 / Accepted: 6 August 2012

Abstract Multiple myeloma (MM) and AL amyloidosis are caused by the expansion of monoclonal plasma cells and secretion of dysproteinemia (Bence Jones protein and free light chain) and some patients require the hemodialysis. Myeloma kidney is mainly caused by the cast nephropathy of the distal tubuli, whereas, AL amyloid-protein is mainly deposited in glomeruli with massive fibrillar involvement. Therefore, almost MM patients presents a symptom of renal insufficiency, whereas, almost patients of AL amyloidosis present a nephrotic syndrome with severe hypoalbuminemia. These two diseases have some similar characteristics such as up-regulation of cyclin D1 gene by 11:14 chromosomal translocation. High-dose chemotherapy supported with autologous peripheral blood stem cells is effective for these two diseases. However, they are still difficult to be cured and require long-term disease control. In recent years, introduction of novel agents has changed their treatment strategies from the palliation therapy to the clinical cure.

Keywords Multiple myeloma · AL amyloidosis · ASCT · Renal insufficiency

This article was presented at the 54th Annual Meeting of the Japanese Society of Nephrology.

K. Suzuki (✉)
Department of Hematology, Japanese Red Cross Medical Center, 4-1-22 Hiroo, Shibuya-ku, Tokyo 150-8935, Japan
e-mail: ken-suzuki@mtb.biglobe.ne.jp

Introduction

Multiple myeloma (MM) is an incurable disease with high incidence rate in the elderly. Responsiveness to treatments varies largely among the patients due to high heterogeneity of MM. Decision of the treatment has been a difficult issue in MM. However, changes can be seen in its treatment strategies since good quality of response can be realistically obtained due to an introduction of novel drugs (bortezomib, lenalidomide, and thalidomide). This article reviews the latest trend and the future perspective of treatment for MM which has advanced remarkably in recent years.

MM and AL amyloidosis are similar diseases resulting from clonal proliferation and dysfunction of plasma cells, in which renal dysfunction due to deposition of immunoglobulin (M protein/amyloid) or other causes are frequently observed. Since exacerbation of renal function is closely associated with the prognosis of patients, maintenance or improvement of renal function by managing the underlying disease is required. In recent years, stratification of myeloma as high-risk and standard-risk by Mayo group has been introduced [1]. Deletion of 17p by FISH, t (14:16), Cytogenetic hypodiploidy, and β2-microglobulin >5.5 and LDH level >upper limit of normal are high risk sign. T (4:14) and cytogenetic deletion 13 are considered as intermediate risk by the reasons of overcoming with new drugs. After that, IMWG stratification is also published; Standard-risk were Hyperdiploidy (45 % of MM mainly IgG type and aged patients), t(11;14)(q13;q32) CCND1↑, and t(6;14) CCND3↑. Intermediate-risk were t(4;14)(p16;q32) MMSET↑ and deletion 13 or hypodiploidy by conventional karyotyping. High-risk were 17p deletion, t(14;16)(q32;q23) C-MAF↑, and t(14;20)(q32;q11) MAFB↑.

Published online: 13 September 2012

We classified AL amyloidosis into four groups as follows; cardiac, renal, gastrointestinal and pulmonary amyloidosis, and the others according to the main organ with AL amyloid materials deposition. In this decade, novel agents (bortezomib, thalidomide and lenalidomide) have become available to treat multiple myeloma in Japan. In this article, we review the recent trend for the diagnosis and treatment strategies of multiple myeloma and AL amyloidosis by focusing on how to improve renal lesion.

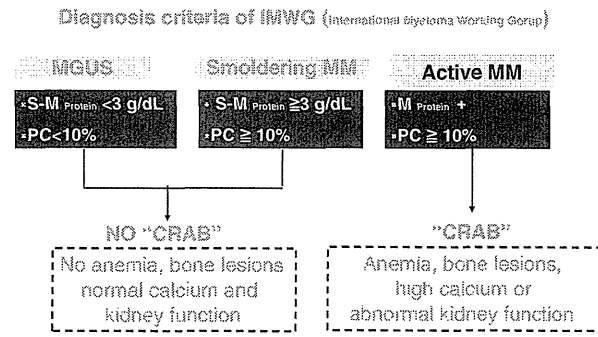

Fig. 1 Diagnostic criteria of IMWG. Anemia, bone lesions, high calcium or abnormal kidney function are called "CRAB". We start any initial treatments at the symptomatic myeloma. MGUS and smoldering myeloma are only careful following

Diagnosis and treatment of multiple myeloma

Historical perspective

In 1962, Bergsagel et al. [2] reported that L-phenylalanine mustard (melphalan) could induce remissions in approximately one third of patients with MM. In 1967, Salmon et al. [3] reported that high doses of glucocorticoids could induce remissions in patients with refractory or relapsing MM. Combination therapy with melphalan and prednisolone in 1969 by Alexanian et al. [4] showed a better result than melphalan alone.

However, the response rate with alkylators and corticosteroids was only approximately 50 %, and CR was rare. Cure was never a goal of therapy as it was assumed unattainable. Instead, the goal was to control the disease as much as possible, providing the best quality of life to patients for the longest duration by judicious, intermittent use of the 2 available classes of active chemotherapeutic agents. Also in 1986, clinical studies evaluating HDT with single ASCT (McElwain) and double ASCT (Barlogie) were conducted. In 1996, the first randomized study showed benefits with HDT with ASCT versus standard chemotherapy. Berenson et al described an efficacy of bisphosphonate pamidronate in reducing skeletal events in patients with advanced MM.

In 1999, thalidomide was introduced and the first nonmyeloablative mini-allogeneic transplants were introduced with several novel agents that target the biological pathway of the disease, as well as long-acting Adriamycin® analogues. In the past decade, thalidomide, bortezomib, and lenalidomide have emerged as effective agents for the treatment of myeloma, producing spectacular results in combination with other known agents in terms of response rate, CR rate, progression-free survival (PFS), and, more recently, overall survival. In 2001, a new classification system introduced "CRAB" features of organ damage (Fig. 1) [5]. In 2004, the International Staging System was introduced. The results obtained from new combinations have indeed been remarkable and have created a relatively new philosophy of treating myeloma with a goal of potential cure rather than disease control.

Chemotherapy is indicated for patients with newly diagnosed symptomatic myeloma, although it is generally not recommended for patients with monoclonal gammopathy of undetermined significance (MGUS), smoldering, or asymptomatic myeloma. Age, performance status, and neurologic and co morbid conditions are critical factors in the choice of initial therapy. Melphalan and prednisone combination can no longer be considered as a standard of care in patients who are 65 years of age or older. Our findings suggest that bortezomib plus melphalan-prednisone is the standard front-line treatment for patients with myeloma who are 65 years of age or older and cannot tolerate more aggressive treatment [6].

During the past decades, high-dose therapy with autologous stem-cell transplantation (HDT-SCT) has become the standard treatment option for patients with untreated multiple myeloma (MM) who are younger than 65 years of age; however, HDT-SCT is not usually recommended for older patients and patients with clinically significant co-morbidities.

A recent study has shown that long-term survival improved significantly in younger patients while only limited improvement was achieved in elderly patients. Improved treatment for such older patients ineligible for HDT-SCT was much-awaited.

Should we treat patients with myeloma with multidrug, multitransplant combinations to pursue the goal of potentially curing a subset of patients, recognizing that the balance of adverse events and effect on quality of life will be substantial? Or should we consider myeloma as a chronic incurable disease with a goal of disease control, using the least toxic regimens, emphasizing a balance between efficacy and quality of life, and reserving more aggressive therapy for later lines?

Induction therapy for newly diagnosed multiple myeloma (NDMM)

Effect of novel agents on outcome in NDMM was dramatically improved (Fig. 2) [7]. Using the combination therapies with new drugs, multiple myeloma (MM) is changing from a incurable disease into either a chronic one or a curable disease.

Bortezomib

Bortezomib IV is an ubiquitin-proteasome inhibitor and indicated for the treatment of MM. Bortezomib is a reversible inhibitor of the chymotrypsin-like activity of the 26S proteasome in mammalian cells. It is cytotoxic to a variety of cancer cell types in vitro and causes suppression in tumor growth in vivo in nonclinical tumor models, including MM. Specifically, bortezomib is effective in MM via its inhibition of nuclear factor-κB activation, its attenuation of interleukin-6-mediated cell growth, a direct apoptotic effect, and possibly antiangiogenic and other effects [8]. Regarding the treatment of patients who are not eligible for transplantation, MPT and MPB have shown significantly better overall survival (OS) benefit than that of MP and are the recommended treatments [6, 9]. The proteasome inhibitor bortezomib has been approved in the USA in 2005 for the treatment of MM patients with a history of at least one prior therapy, based on results from the phase III APEX study which showed superiority of bortezomib over high-dose dexamethasone in patients with relapsed MM [10]. The majority of treatment guidelines currently recommend incorporating HDT/SCT into initial therapy programs for patients who are 65 years of age or younger and to consider such a therapy for patients 60–70 years of age with good performance status and a lack of co morbid illnesses since HDT/SCT provides the highest chance of inducing a complete remission. However, even when patients achieve CR, the vast majority of patients will ultimately relapse. The standard frontline therapy for patients who are 65 years of age or older, and for patients who are not likely to proceed to HDT/SCT, consists of oral MP at doses similar to those used in this study. Combination therapies such as MP (at a dose of 0.25 mg/kg/day) are given orally at doses used for 4 consecutive days every 6 weeks, showed superior survival versus melphalan alone. With MP therapy, an OR rate of approximately 50 %, a CR rate of 2 to 5 % and a median time to response of 3–5 months have been historically reported [4].

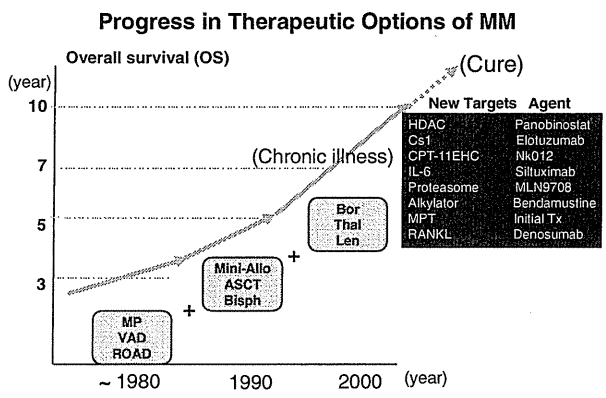

Fig. 2 Effect of novel agents on outcome in newly diagnosed myeloma. Overall survivals were elongated by the effect of HDT with ASCT from 1994, longer due to new drugs from 2001. 1970, MP; 1986, HDT with ASCT; 1999–2000, new drugs (bortezomib, lenalidomide, and thalidomide) were epoch making. The CS-1 antibody (elotuzumab) and IL-6 antibody (siltuximab) may be effective with some combinations. Bendamustine, a bifunctional agent, shares properties of alkylating agents and purine analogs. New combination trials of new agents, as shown in right-side may be promising

Final results of the phase 3 VISTA trial

Recently 5 year OS follow up data has been published. The data indicates that OS in MPB with 60.1 months follow-up is significantly superior to that of MP. The OS of MP-B and MP were 56.4 months (13.3 months improvement) and 43.1 months respectively. This data is very much remarkable because the OS improvement was 13.3 months although even MPT could improve only 6.6 months in its meta analysis. As a result of this VISTA study, MPB became the standard treatment for untreated transplant in-eligible patients [11].

To evaluate safety, pharmacokinetics (PK) and efficacy of bortezomib combined with melphalan and prednisolone (MPB) therapy, we conducted a phase I/II study for untreated Japanese MM patients who were ineligible for hematopoietic stem cell transplant (HSCT). This was a dose-escalation study designed to determine the recommended dose (RD) of bortezomib in combination with melphalan and prednisolone by evaluation of the maximum tolerated dose based on dose-limiting toxicity (DLT) in the phase I portion, and to investigate the overall response rate (ORR; CR + PR) and safety of MPB therapy in the phase II portion. Particularly, a continuity of treatment cycles was historically compared with a global phase III study (VISTA trial), and the incidence of interstitial lung disease was assessed. This phase I/II study in Japan suggests that the RD of bortezomib in MPB therapy is 1.3 mg/m^2 and the MPB therapy in newly diagnosed Japanese MM patients ineligible for HSCT is as effective as that shown in VISTA trial. Further investigation is necessary to confirm the appropriate administration schedule of this combination in Japanese patients [12].

International uniform response criteria

	PR	VGPR	nCR	CR	sCR
Serum Protein Electrophoresis	≧50%	≧90%	0	0	0
Urine Protein Electrophoresis	≧90%	< 100mg/24h	0	0	0
Bone Marrow Plasma Cells	—	—	<5%	<5%	<5%
Bone Marrow Immunofluorescence	—	—	—	—	Negative
Serum/Urine Immunofixation	—	—	Positive	Negative	Negative
Serum Free Light Chain Ratio	—	—	—	—	Normal

Durie BGM, et al. Leukemia 20:1467-73, 2006.

Fig. 3 International uniform response criteria. Serum protein electrophoresis, serum/urine immunofixation, and serum free light chain ratio are important

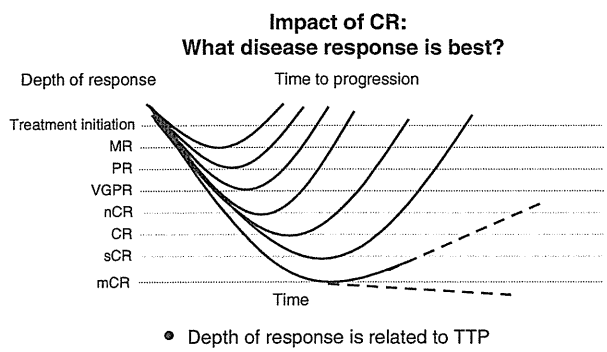

Fig. 4 Impact of CR: depth of response is related to TTP. CR is the surrogated marker for the long survival

What should be the goal of treatment in multiple myeloma? If cure is the goal, then CR is the critical first step (Fig. 3) [13]. CR is a treatment goal in many hematological malignancies, eg- AML, ALL and lymphomas. In the past, achievement of CR in MM was rare. New treatments can increase the rate of CR to the similar level with high-dose therapy followed by ASCT (Fig. 4) [14–16]. Also, CR rate in Phase 3 trials in non-transplant patients was: MPB 30 %; MPT 2-16 %; MPR 13 %; MPR-R 18 %, and long term RD 22 %. MM may not be a single disease cytogenetically; achievement of CR seems particularly important in the 15 % of patients with high-risk MM, since survival is similar in patients without high-risk features who have and have not achieved CR [6, 17–20].

Cyclophosphamide and thalidomide

Cyclophosphamide has been added to thalidomide and dexamethasone (CTD) with excellent response rates among newly diagnosed MM patients who received subsequent SCT, with higher response rates seen after SCT.

The combination in 3-weekly schedules of cyclophosphamide (50 mg PO or 300 mg/m^2 PO weekly or 150 mg/m^2 d1–5), thalidomide (200–800 mg daily, increasing doses or intermittent administration 400 mg d1–5 and d14–18) and dexamethasone (40 mg per day for 4 days) (CTD) results in an ORR of around 60 %, a median TTP of 10–12 months and a 2-years PFS of 57 % [21–23].

Comprehensive reviews on the use of thalidomide have been published and include efficacy and safety in relapsed MM. The rationale for using thalidomide was based on its antiangiogenic properties because, in MM, increased microvessel density has been inversely correlated to survival. However, thalidomide has multiple modes of action, including immunomodulatory effects. This initial experience generated a great enthusiasm, and a large number of phase II trials were rapidly conducted. A systematic review of such 42 trials on >1600 patients confirm that the response rate is 29 % with an estimated 1-year overall survival (OS) of 60 %. The well-known teratogenicity of thalidomide is not a major concern in patients with MM because of patients age, but justifies careful informing of patients and programs to avoid drug exposure in women with childbearing potential. The major toxicities of thalidomide are fatigue, somnolence, constipation, and mostly peripheral neuropathy, which are related to the daily dosage and to treatment duration. The overall incidence of peripheral neuropathy is 30 % but may be higher if treatment is prolonged for >1 year. Because this complication may be disabling and sometimes irreversible, patients should decrease the dose or stop the treatment if significant numbness occurs.

After induction treatment, two to four cycles of combination therapies is followed by the maintenance therapy, which is continuous therapy with a single agent, with reasonable balance between maximum benefits and minimum toxicities [24] until the time of disease progression.

Maintenance therapy for multiple myeloma

I prefer disease control as a treatment goal, except in selected high-risk patients in whom an aggressive approach to achieving CR may be the only option to long-term survival (Fig. 5). The disease control approach involves targeting very good partial response (minimal residual disease) rather than CR as a goal by using limited, less intense therapy first and moving to more aggressive approaches as need arises (sequential approach): this allows patients to help determine the timing and number of transplants.

Post-transplant consolidation/maintenance with novel agents can become an important step forward. Thus, it has recently been reported that post-transplant consolidation with thalidomide, lenalidomide or bortezomib increases the CR rate. In this regard, it has been shown that post-ASCT consolidation with VTD can induce long-lasting molecular remission [25, 26]. Thalidomide maintenance prolonged the OS in two transplant series [27].

The response rate to treatment with single-agent thalidomide in patients with relapsed and/or refractory MM is between 30 and 40 % [28].The response rate increases from 50 to 65 % when thalidomide is combined with dexamethasone with or without cytotoxic agents.

The cure-versus-control debate is hot. Indeed, CR is a surrogate marker for improved OS. However, for the majorities of MM patients, the disease control approach (Maintenance therapy) involves targeting very good partial response (VGPR) rather than CR as a goal. This is a pilot study of the prospective, sequential registered trial of the

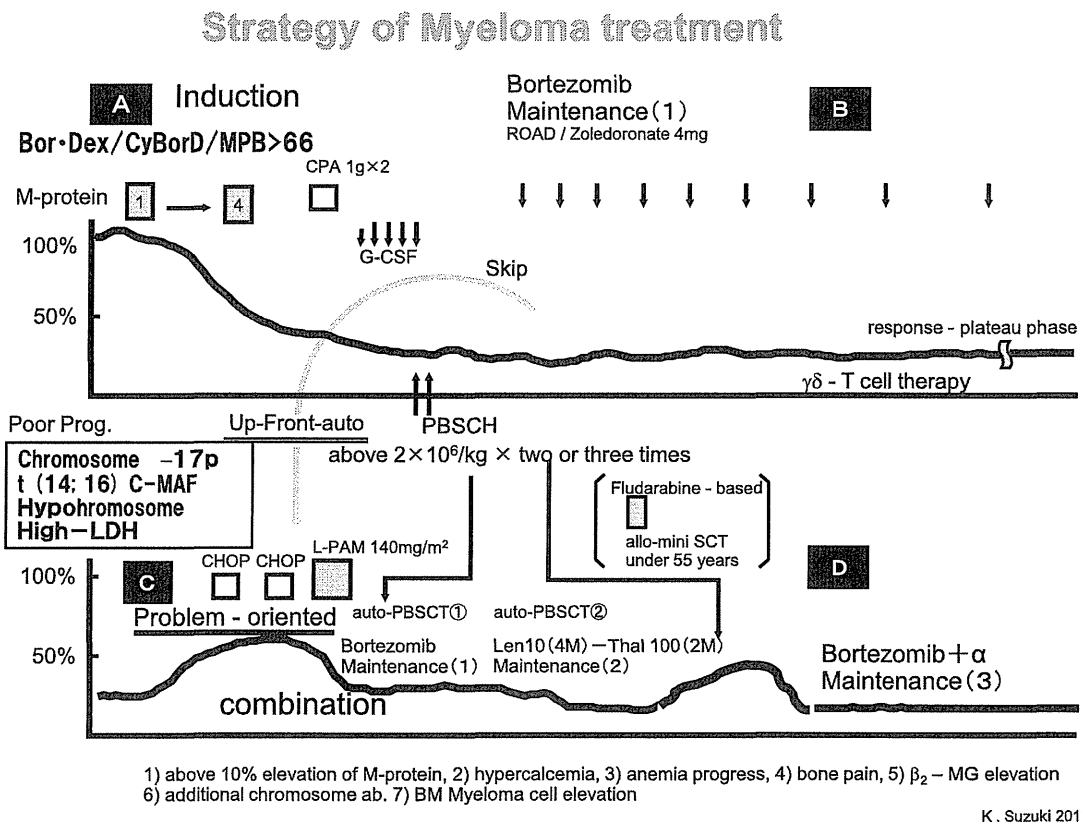

Fig. 5 Strategy of myeloma treatment in our institute. We divided in four phases: initial therapy by two to four courses of BorDex/CyBorD/ or MPB >66 years old followed by PBSC-harvest. If the high risk patients, up-front PBSC-transplantation followed by Bor-maintenance. Otherwise, if the standard risks patients, maintenance-therapies may be the B-stages until progress disease. PD are defined as (1) above 10 % elevation of M-protein, (2) hypercalcemia, (3) anemia progress, (4) bone pain, (5) β_2-MG elevation (6) additional chromosome ab. (7) BM myeloma cell elevation. After PD, problem-oriented PBSCT may be done with second maintenance with Lenalidomide

significance of BD maintenance therapy for long-term survival with good QoL.

From September 2008, we continued exploratory study of effects of bortezomib on the ability of patients with relapsed, refractory multiple myeloma to continue maintenance therapy [29] (Clin. Eth. No: JRC 170). Bortezomib had been associated with fatal lung disorders, with a high number of reported cases in Japan. Post-marketing surveillance, however, showed a low incidence of 3.6 %. Peripheral neuropathy (20–30 %) is a major concern. Informed consent was obtained from 43 patients with a mean prior treatment (e.g., VAD, ROAD, ASCT) history of 23 months, PS $\leq$2, and no significant organ lesions. Efficacy of bortezomib as maintenance therapy in patients achieving VGPR/PR with remission induction therapy has not been investigated. This study of bortezomib maintenance therapy in patients achieving VGPR/PR with bortezomib is therefore investigating the effects of treatment on patients ability to continue maintenance therapy and adverse drug reaction incidence. There were 11 cases of karyotypic abnormalities (35 %) with 8 cases of complex abnormalities. Patients received dexamethasone (20 mg/body) daily for 2 days every 2 or 4 weeks with bortezomib, 1.3 mg/m^2 div. Time-to-progression (TTP) was the primary efficacy endpoint (Fig. 6) [29]. The adverse reactions of BD maintenance include asthenia conditions, peripheral neuropathy, thrombocytopenia were all G-1 and well tolerated. Long-term survival with good QoL is the most important goal for the elderly/low genetic risk MM patients. BD maintenance is good available for this group (24/43 cases) over 20 months (Fig. 7), especially in the cases of total delivery dose over 40 mg. However, the other group of patients (8/33 cases) in rapidly relapsing with complex karyotypic abnormalities may need the strong combination chemotherapy.

Recently, lenalidomide maintenance therapy improved median progression-free survival (41 vs. 23 months with placebo; hazard ratio, 0.50; $P < 0.001$) [30].

Therapy for relapsed or refractory multiple myeloma (RRMM)

Progressive disease is defined as follows: (1) Above 25 % elevation of M-protein, (2) hypercalcemia: corrected serum calcium >11.5 mg/dL, (3) the absolute increase of free light chain (FLC) must be >10 mg/dL, (4) definite development of new bone lesions or soft tissue plasmacytomas, (5) decrease in hemoglobin of >2 g/dL, (6) rise in serum creatinine by 2 mg/dL or more, (7) increase of BM myeloma cell above 10 %.

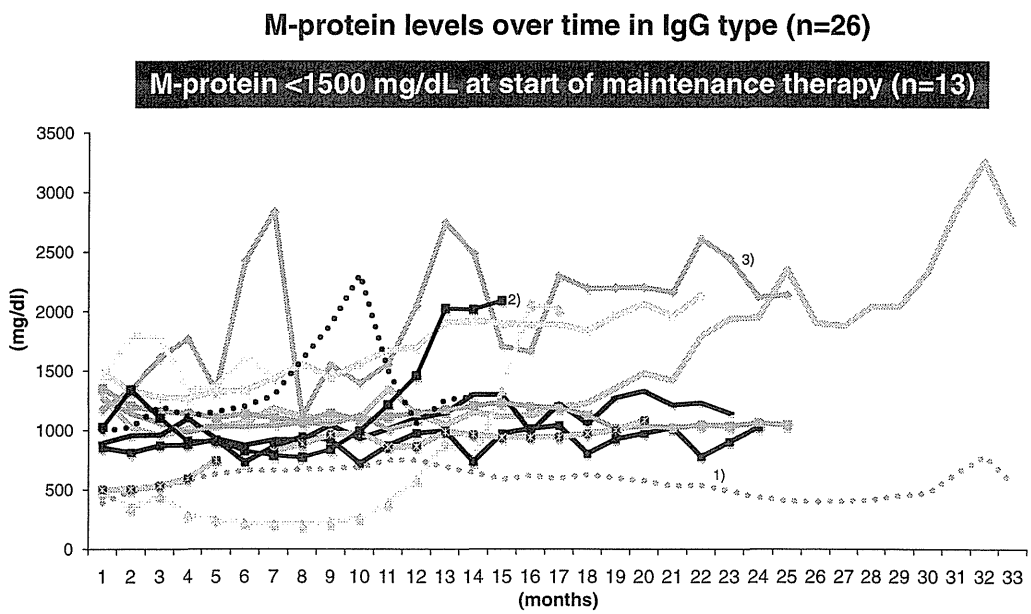

1) 46,XX,t(11;14)(q13;q32)[1]/46,XX[29] 2) 50,add(X)(q28),-X,-1,+3,+7,-8,+9,+15,del(22)(q139,+3mar,inc[cp12]/46,XX[18]
3) 83~85,XX,-X,-X,der(1;2)(q10;q10)- 2,-2,-2,-3,add(3)(p2?),-4,-4,add(4)(p16),add(4)(p16),-5,-5,-6,-6,-8,add(10)(q22)2,-13,-13,-13,del(13)(q?),- 14,-15,-16,-16,-16,-17,add(18)(q23)×2,+14 ~ 15mar,inc[cp2]/

Fig. 6 Maintenance therapy with bortezomib for the VGPR IgG-myeloma patients. Monthly administration of bortezomib are effective as the stabilization of M-protein levels over time in IgG type ($n = 26$). It needs 20 months average until PD. However, high risk group are difficult to control in this manner

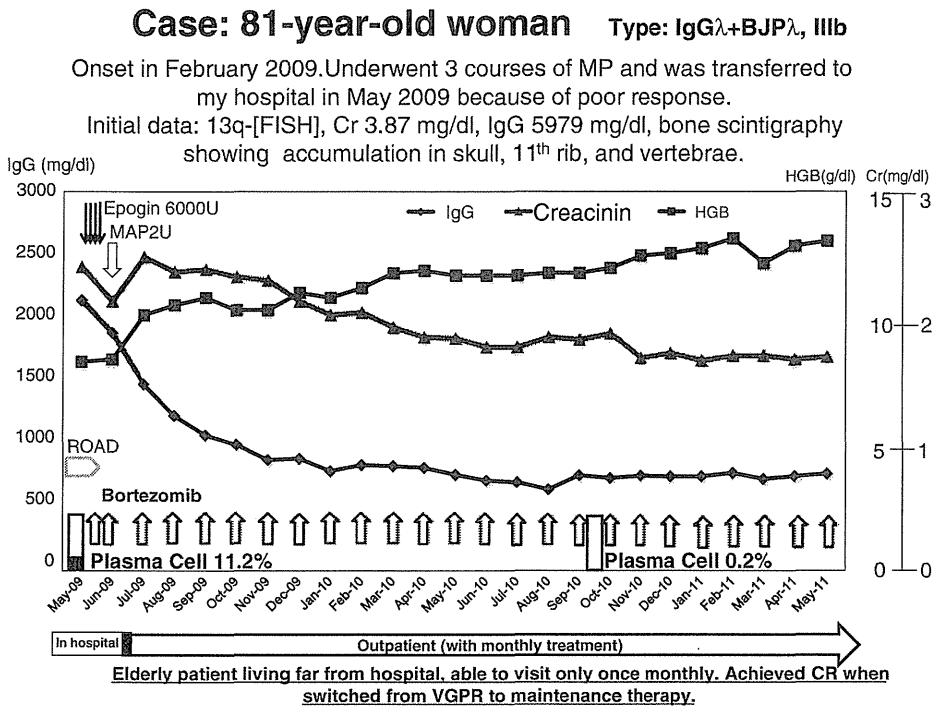

Fig. 7 A case of Bor-maintenance therapy. Elderly patient (81 year old female: IgGλ + BJPλ, stage IIIb) living far from hospital, can visit only once monthly. After 14 months therapy, she achieved CR when switched from VGPR to maintenance therapy

Analysis of second primary malignancies (SPM)

Another important issue in MM is risk of developing SPMs due to living longer from diagnosis. Population studies show MM patients have increased risk of specific SPMs following initial diagnosis, notably acute myeloid leukemia (AML). Some MM therapeutic agents are particularly associated with elevated risk of SPMs. Melphalan is associated with increased risk of secondary acute leukemia. There were imbalances in SPM incidence, including myeloid and lymphoid leukemias, with post-transplant lenalidomide maintenance therapy and with MP-lenalidomide. Persistent significant OS benefit with VMP versus MP; 13.3-months increase in median, and MPT versus MP increase 6.6 months [9].

Secondary malignancies and lenalidomide: by summarizing the data to-date, the incidence of all/invasive SPM is significantly increased in Lenalidomide arms, driven by hematologic SPM ($P < 0.001$). B-ALL, Hodgkin lymphoma is reported in post high-dose melphalan and ASCT setting. Sensitivity analysis (including SPM as an event) demonstrates negligible PFS differences. The overall benefit–risk profile of lenalidomide in NDMM remains positive [31, 32]. Risk Factors for Secondary Malignancies Treatment with lenalidomide may be treatment duration >24 months, male, age >55 years, ISS stage III, previous DCEP (role of concomittant or previous exposure to alkylators?) induction by univariate and multivariate analysis in IFM 2005.

In Japanese SPM Report by JRCMC, retrospective analysis for 325 MM patients from 1998 to 2010 (13 years) showed t-MDS/AML developed 17 (5.2 %) patients. Median time to onset: 52 months in t-AML and months in t-MDS. All the patients with t-AML died in a short time, suspected to be treated with Melphalan, and no patients had been given Lenalidomide. We have to select chemo regimen taking into account the risk of t-MDS/AML [33].

Renal dysfunction in multiple myeloma

Timing of treatment initiation in multiple myeloma is depending on existence of organ dysfunction. Usually when any symptom such as bone symptoms, renal dysfunction, anemia, or hypercalcemia is observed, it is diagnosed as symptomatic multiple myeloma and treatment should be started. Renal dysfunction in multiple myeloma is one of the complications that require the most careful attention and occurs via various mechanisms. Of these, the most frequent case is cast nephropathy, also known as myeloma kidney, in which excessive light chains of M protein (BJP) secreted by proliferated plasma cells form cast by depositing themselves in renal tubules. In addition, hypercalcemia associated with osteolysis by myeloma cells, deposition of amyloid in glomeruli, hyperviscosity syndrome, hyperphosphatemia, renal infiltration of myeloma cells are also the causes of renal dysfunction. Other than those, care must be given to recurring urinary tract infection, drugs, dehydration that may act as exacerbation

factor. According to the statistics of Japanese Society of Myeloma [34], approximately 15 % of newly diagnosed multiple myeloma patients have complication of renal dysfunction and the rate increases as the disease progresses. Bence Jones protein (BJP) type and IgD type of myeloma that excrete high amount of Bence Jones protein into urine show high frequency of renal dysfunction. In 197 patients diagnosed as multiple myeloma during 12 years (1995–2006) in our facility, 3.6 % of IgG type and 8.9 % of IgA type showed higher than 2 mg/dL of creatinine on the first visit, were whereas BJP type accounted for 36.8 % (Fig. 8). Because renal dysfunction becomes irreversible if timing of treatment is missed, immediate treatment is necessary. It is reported that renal dysfunction remains reversible when serum creatinine is below 4 mg/dL, Ca is below 11.5 mg/dL and urine protein is 1 g/day or lower [35]. Although these are the data before introduction of novel agents, in the 423 patients with newly diagnosed multiple myeloma, patients with renal dysfunction (22 %) showed significantly shorter survival time compared to the patients with normal renal function (8.6 vs. 34.5 months). In addition, Blade et al. reported that in the same patients with reduced renal function, those who recovered their renal function by subsequent chemotherapy showed significantly extended survival time compared to those without recovery of renal function (28.3 vs. 3.8 months). Therefore, although renal dysfunction in multiple myeloma is a poor prognostic factor, good prognosis can be expected if the treatment restores renal function. For this, it is important to restore renal function by implementing effective treatment in patients with renal dysfunction before it becomes irreversible and requires hemodialysis. In the multiple myeloma patents in our facility mentioned above, hemodialysis was introduced to eight out of 197 cases.

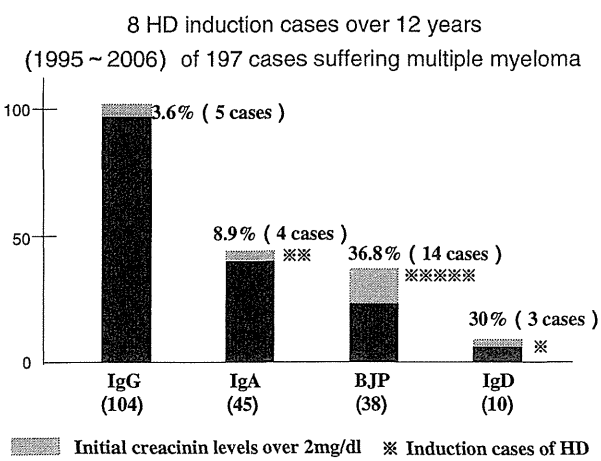

Fig. 8 HD induction cases suffering MM. Initial creatinine levels over 2 mg/dL were 10–20 %, mainly in BJP and IgD type. HD induction was also frequent in these populations

Improvement of renal function and treatment strategy for multiple myeloma

Improvement of the primary disease is the basic remedy of renal dysfunction that complicates with multiple myeloma. Since 2005, treatment strategy for multiple myeloma has significantly changed due to the successive introduction of novel agents. The three drugs including a proteasome inhibitor bortezomib, and two immunomodulatory drugs (IMiDs), lenalidomide and thalidomide, are referred to as novel agents, and each drug has characteristic profiles of efficacy and safety. While all those agents can be expected to restore renal function due to improvement of the primary disease, bortezomib, with strong antitumor effect, is reported to rapidly improve renal function (Fig. 9). Roussou et al. retrospectively compared improvement of renal function among traditional chemotherapy group, IMiDs (lenalidomide or thalidomide)-based treatment group, and bortezomib-based treatment group with 96 cases of newly diagnosed multiple myeloma. It showed that the best and the most rapid improvement of renal function were observed in the bortezomib-based treatment group. Renal response rate (minor response and better) based on creatine clearance improvement and time to response as 59 % and 1.8 months in chemotherapy group, 79 % and 1.6 months in IMiDs-based group, and 94 % and 0.69 month in bortezomib-based group, respectively [36]. In addition, some cases with withdrawal from dialysis are also reported. Thus, administration of bortezomib should be considered in patients with acute or severe renal dysfunction if it is possible.

Lenalidomide

Lenalidomide is an anti-myeloma drug possessing dual functions of antitumor effect and immunomodulating activity. Because lenalidomide is urinary excreted, its blood concentration increases in patients with renal dysfunction which leads to high incidence risk of adverse reactions [37]. However, lenalidomide itself has no renal toxicity and clinical studies showed improvement of renal function in the patients treated with lenalidomide. Lenalidomide can be administrated by proper adjustment of its dose corresponding to renal function according to the package description [38]. In fact, it is reported that adjusted dosing of lenalidomide to patients with renal dysfunction resulted with similar anti-myeloma efficacy to those with normal renal function [39, 40], and recovery of renal function was also observed [41]. Similar to bortezomib, cases that withdrew from dialysis are reported [42].

Renal Response	CC-based regimen (n=32)	IMiDs-basede regimen (n=47)	Bortezomib-based regimen (n=17)
CR renal	41%	45%	71%
	47%	45%	82%
≧MR renal	59%	79%	94%
Time to Response	1.8 months	1.6 months	0.69 months

M. Roussou et al.: Leukemia Research 34, 1395–1397, 2010

Stages		GFR (ml/min/1.73 m²)
1	Kidney damage with normal or elevated GFR	Over 90
2	Kidney damage with mild reduction of GFR	60-89
3	Moderate reduction of GFR	30-59
4	Severe reduction of GFR	15-29
5	Renal failure	Below or Hemo Dialysis

Response	Baseline eGFR* (ml/min/1.73 m²)	Best CrCl Response (m l /min)※
CR renal	<50	≥60
PR renal	<15	30-59
MR renal	<15	15-29
	15-29	30-59

※At least keep 2 months

Meletios A. dimopoulos et al.: Journal of Clinical Oncology

Fig. 9 Complete response (CR) renal. CR may be attained by bortezomib-based regimen not only the high levels percentage but also time to response. 5-stage is divided as the figure

Stratified analysis of lenalidomide/dexamethasone therapy by age showed similar efficacy and tolerability in elderly (over 65 years of age) to those of youth [43]. Hence this therapy is considered to be useful especially for elderly patients with renal dysfunction if the dose is properly adjusted corresponding to the renal function. Thalidomide does not require dose control depending on renal dysfunction, but it has not been reported in large studies that thalidomide is effective on the improvement of renal function. In any case, early diagnosis and timing of initiation of treatment are important. In addition, full understanding of efficacy and safety profiles of novel agents and using them in combination with existing drugs appropriate for individual patients are the basis of treatment strategy.

Diagnosis of AL amyloidosis and renal dysfunction

AL amyloidosis is a disease with poor progression in which deposition of amyloid causes multiple organ failure. Amyloid consists of immunoglobulin light chains secreted from monoclonal proliferated plasma cells. Its relative disease MM is often complicated with AL amyloidosis. In spite of the fact that it has the same chromosome translocation such as t (11:14) to MM, it shows different pathological condition (Fig. 10). This may be due to slight difference of translocation breakpoint between AL amyloidosis and MM. However, the disease mechanism remains unknown.

It is classified to cardiac, renal, gastrointestinal, and pulmonary amyloidosis depending on the main organ with amyloid deposition. The symptoms vary and the most common cause of death is cardiac failure. The diagnosis is based on confirmation of amyloid deposition in the involved organs. When AL amyloidosis is suspected in patients with clinical findings such as general malaise, edema, heart failure, tubercle in margin of tongue, and skin nodule with stigma, biopsy of organs should be first conducted to confirm deposit of amyloid (Fig. 11). Amyloid is positive with Congo red stain and has positive signal under polarized light with the polarizing filters. AL amyloidosis is definitely diagnosed by confirming monoclonal proliferation of plasma cells through identification of M protein and/or staining pattern of cell surface antigens in addition to deposition of amyloid. Low detection sensitivity of M protein even in immunofixation in AL amyloidosis has been a problem so far. However, the free light chain (FLC) assay that has listed itself in insurance coverage in 2011 in Japan, allows over 90 % detection and is reported to be effective in diagnosis. Amyloid deposits are predominantly composed of amyloid fibrils which are very stable structures with a common cross core fold. Deposits are always rich in proteoglycans and glycosaminoglycans, some of which are tightly associated with the fibrils and further

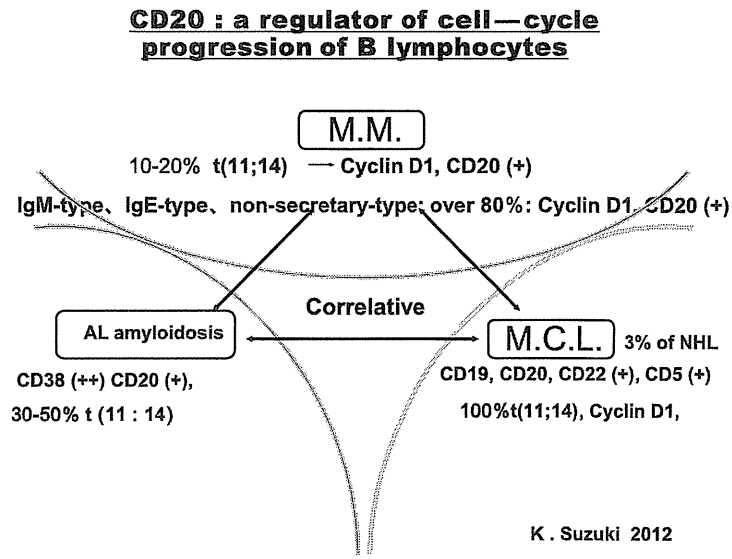

Fig. 10 Correlation of pathogenesis between MM, AL amyloidosis and Mantle cell lymphoma by the up-regulated cyclin D1 function. Mantle cell lymphoma is high tumor growth with 100 % t (11:14), MM have 10–20 % t (11:14) with moderate growth and secretary Ig functions. Some strange and rear MM patients (i.e. IgM-type, IgE-type, non-secretary-type) showed translocation 11:14 over 80 %. Otherwise, AL amyloidosis showed 30–50 % t (11:14). There may be the differences of break points on the translocation foci

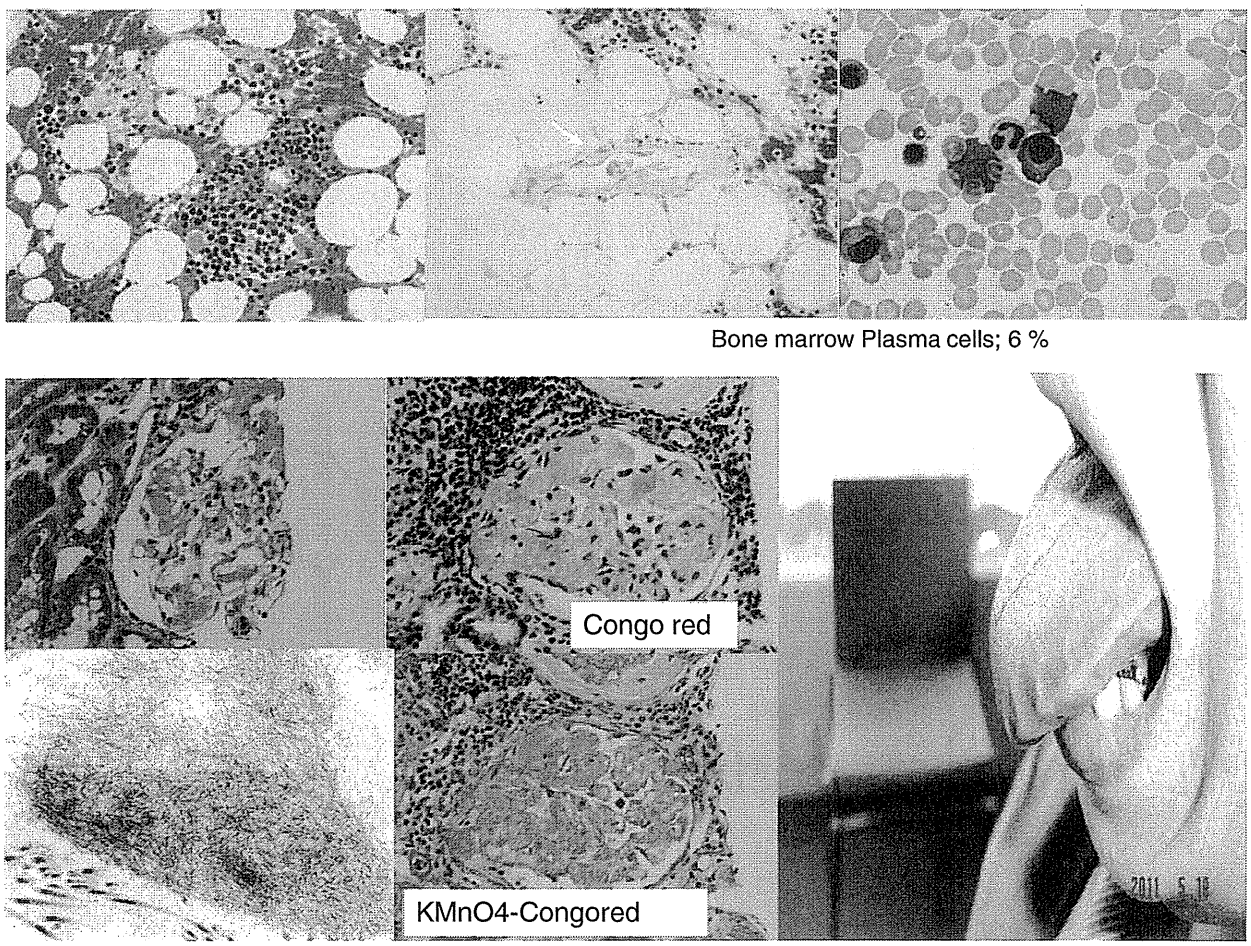

Fig. 11 Histology of bone marrow and kidney. Tubercle in margin of tongue is important finding for diagnosis. The amyloidogenic plasma cell clone is mature type mainly CD19 negative clone. We can see amyloid deposition in blood vessels of bone marrow in some cases. Congo-red staining and amyloid fibrils by EM is important by the low detection with light chain staining